

# Dominance of Charge-Assisted Hydrogen Bonding on Short Contacts and Structures that Crystallize with $Z' > 1$

Kirsty M. Anderson,<sup>†</sup> Andrés E. Goeta,<sup>†</sup> Jessica E. Martin,<sup>†</sup> Sax A. Mason,<sup>‡</sup> Garry J. McIntyre,<sup>†,‡</sup> Benedict C. R. Sansam,<sup>†</sup> Clive Wilkinson,<sup>†</sup> and Jonathan W. Steed<sup>\*†</sup>

<sup>†</sup>Durham University, Department of Chemistry, South Road, Durham, DH1 3LE, U.K.

<sup>‡</sup>Institut Laue-Langevin, 6 Rue Jules Horowitz, BP156, 38042, Grenoble, France

 Supporting Information

**ABSTRACT:** An enantiotropic pair of polymorphs of  $(H_2\text{-}o\text{-PDA}^{2+})_4(H_5O_2^+)(SO_4^{2-})_4(HSO_4^-) \cdot 2H_2O$  (**1**) interconvert at 140–142 K with a concomitant change in  $Z'$ . The details of the structural change are studied by single-crystal X-ray and neutron diffraction which shows that both forms are close packed with the difference resulting from the linearization of hydrogen bonds at low temperature as part of an extensive charge-assisted hydrogen-bonding network. The related  $(H_2\text{-}o\text{-PDA}^{2+})_2(SO_4^{2-})_2 \cdot 3H_2O$  (**2**) has also been characterized by single-crystal neutron diffraction and exhibits a disordered “flip-flop” water chain and short nonbonded O···O contacts enforced by  $NH_3^+ \cdots OSO_3^{2-}$  hydrogen-bonded bridges. A total of seven other related salts have been isolated and structurally characterized revealing a surprisingly high incidence of  $Z' > 1$  structures as a result of frustration in the charge-assisted hydrogen-bonded network.

## ■ INTRODUCTION

Structures that crystallize with  $Z' > 1$ , that is, more than one molecule in the asymmetric unit, are of interest in many areas of crystal engineering and crystal nucleation studies,<sup>1–7</sup> not least in the burgeoning field of crystal structure prediction where the ability to predict whether a given molecule is likely to crystallize with high  $Z'$  can narrow the initial search criteria, offering large computational advantages.<sup>8–10</sup>

Structures that crystallize with high  $Z'$  are also of interest in the field of crystal growth, and indeed there has been considerable debate surrounding the phenomenon, particularly whether all structures with  $Z' > 1$  are just metastable forms of known or undiscovered thermodynamically stable  $Z' = 1$  polymorphs.<sup>3</sup> This suggestion presupposes that for all structures with  $Z' > 1$  there is a lower energy  $Z' = 1$  form waiting to be discovered, but it is hard to imagine that this postulate is true across all structures particularly when considering concepts such as frustration,<sup>11</sup> and the fact that in some known polymorphic compounds  $Z' > 1$  forms have been shown to be more stable than their  $Z' = 1$  counterparts.<sup>12</sup> It is also possible that enantiotropic systems exist in which the stability order of  $Z' = 1$  and  $Z' > 1$  polymorphs changes as a function of temperature.

Polymorphism where the polymorphs have different values of  $Z'$  are not common but do exist.<sup>13</sup> In the majority of cases we have identified, polymorphs with different  $Z'$  values are obtained using different crystal-growth conditions or media. There are also some structures where the value of  $Z'$  is dependent on temperature, although there has been some discussion on whether these should be referred to as polymorphic transitions or modulated structures.<sup>14</sup> The structural effects arising from phase transformations where  $Z'$  is modified range from changes in conformation such as in 9-phenylfluoren-9-ol 4-methylcyclohexylamine clathrate<sup>15</sup> (where the low-temperature  $Z' = 3$  form undergoes a

second-order phase transition at 232 K to a higher-temperature  $Z' = 1$  form accompanied by a small change in the host conformation) to more subtle effects such as in 1-hydroxy-1,1,3,3-pentaphenyldisiloxane<sup>16</sup> where there is a phase transition observed between 100 and 150 K from  $Z' = 2$  to  $Z' = 4$  as increased thermal motion of the coordinated phenyl groups lowers the long-range symmetry of the structure. A range of other subtle temperature-dependent structural transformations have also been studied that do not necessarily result in a change in  $Z'$ . Examples include proton transfer, as exemplified by the work on acid-dimer systems by Wilson and co-workers<sup>17</sup> where temperature changes lead to movement of the proton across the centrosymmetric acid-dimer motif.

We have shown that the combination of a molecule with a resolved chiral center and a strongly directional supramolecular synthon with a preference for centrosymmetry leads to frustrated structures where in order to preserve the dimer motif more than one crystallographically independent molecule must be present in the asymmetric unit unless the system can adopt a less efficient  $C_2$  packing mode.<sup>18</sup> The percentage of structures crystallizing with  $Z' > 1$  in systems like this is as high as 75%, compared to the 8.8% for the Cambridge Structural Database (CSD)<sup>19,20</sup> as a whole. In addition to conflicts between molecular properties such as chirality and the formation of robust supramolecular synthons, competing intermolecular interactions can also result in crystallization with  $Z' > 1$ . We have shown that there is a marked tendency toward decreased-symmetry structures for molecules engaged in more than one competing intermolecular interaction and have observed the proportion of structures

**Received:** June 14, 2011

**Revised:** September 27, 2011

**Published:** September 27, 2011

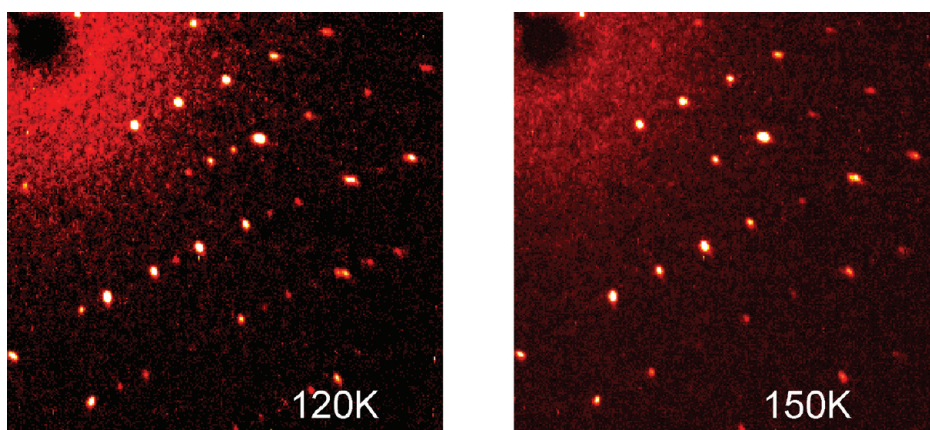


**Figure 1.** Portions of two X-ray diffraction patterns of **1** at 120 and 150 K clearly showing the additional diffraction spots at 120 K due to doubling of the *c* axis.

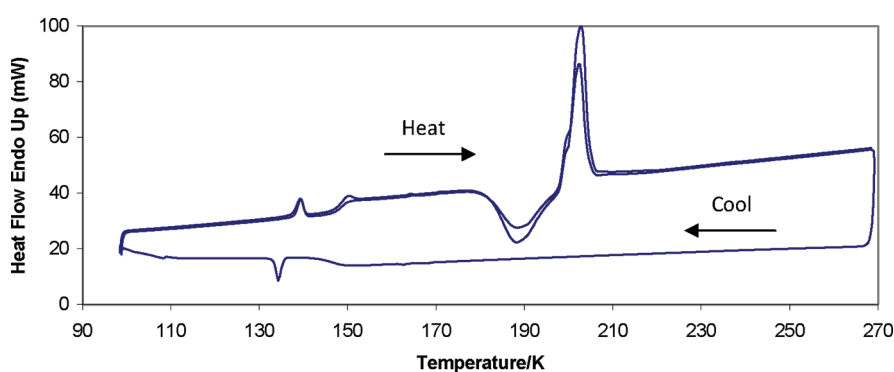


**Figure 2.** DSC trace of **1** showing endotherm corresponding to the phase transition (138 K), glass transition, and large crystallization followed by melting endotherm (180 K) due to surface sulfuric acid solution.

crystallizing with  $Z' > 1$  to be more than 50% in some such cases.<sup>11</sup> In both of these examples, it is likely that any alternative  $Z' = 1$  structure would not be optimized in terms of the intermolecular interactions involved and hence would be less stable.

We have studied the frustration concept extensively in our investigations into a series of aromatic polyamine salts where frustration between strongly hydrogen-bonded networks and  $\pi-\pi$  stacking leads to structures with higher  $Z'$ .<sup>21</sup> This frustration is particularly evident in the structure of the mixed sulfate/hydrogen sulfate salt of doubly protonated *o*-phenylenediamine,  $(\text{H}_2\text{o-PDA}^{2+})_8(\text{SO}_4^{2-})_6(\text{HSO}_4^-)_4 \cdot 8\text{H}_2\text{O}$  (**1**) which crystallizes with  $Z'' = 26$  (i.e., 26 independent molecules or ions in the asymmetric unit)<sup>22</sup> including eight independent cations. Despite the large value of  $Z''$ , the value of  $Z'$  is formally 2 as the smallest integer formula unit is  $(\text{H}_2\text{o-PDA}^{2+})_4(\text{SO}_4^{2-})_3 \cdot (\text{HSO}_4^-)_2 \cdot 4\text{H}_2\text{O}$ .<sup>23</sup> In this structure the sulfate, hydrogen sulfate, and water molecules form a strongly hydrogen-bonded three-dimensional (3D) network around the  $\text{H}_2\text{o-PDA}$  molecules; however, the X-ray data collected on the structure were not of sufficient quality to explore fully the hydrogen-bonded network.

In this paper we explore the effect of temperature on the hydrogen bonding observed in **1** and study the resulting proton transfer in more detail using variable-temperature neutron diffraction. We also explore the frustration concept further by altering both the anion and the cation in seven new compounds

related to **1** to see the effect of changing charge, hydrogen-bonding strength, and molecular shape on the supramolecular synthon formation in these systems.

## ■ RESULTS AND DISCUSSION

**Polymorphism in  $(\text{H}_2\text{o-PDA}^{2+})_4(\text{SO}_4^{2-})_3(\text{HSO}_4^-)_2 \cdot 4\text{H}_2\text{O}$ .** Crystals of compound **1** were grown by recrystallizing *o*-phenylenediamine from aqueous sulfuric acid solution. The resulting crystals exhibit a structure with eight crystallographically independent *o*-phenylene diammonium cations and formally  $Z' = 2$  at 120 K in which the sulfate, hydrogen sulfate, and water molecules form an extended 3D network encapsulating the  $(\text{H}_2\text{o-PDA}^{2+})$  cations.<sup>21</sup> In more detailed studies, we find that compound **1** undergoes a first-order phase transition between 140 and 142 K corresponding to halving of the *c* axis and hence halving of  $Z'$  (from 2 to 1) as the temperature is increased. This phase change was initially monitored by X-ray techniques. The doubling of the *c* axis is shown by the increased number of diffraction spots at low temperature in Figure 1.

The observed phase change was confirmed by differential scanning calorimetry (DSC) (Figure 2) which shows an endotherm with an onset temperature of 138 K corresponding to the  $Z' = 2$  to  $Z' = 1$  transition (apparent  $\Delta H = 1.38 \text{ kJ mol}^{-1}$  without correction for sulphuric acid, *vide infra*) and corresponding exotherm on the cooling scan. The fact that the phase change

**Table 1.** X-ray Data for Compounds 1 (Before and after Phase Change) and 2

	1(LT)	1(HT)	2
T/K	120	140	120
a/Å	7.5186(3)	7.5904(4)	26.969(4)
b/Å	27.5580(12)	27.7714(15)	9.5669(13)
c/Å	19.1638(8)	9.6134(5)	7.5309(10)
β/°	91.615(1)	91.753(1)	93.165(2)
space group	P2 <sub>1</sub>	P2 <sub>1</sub>	P2 <sub>1</sub> /c
Z'/Z''	2, 26	1, 13	1, 7
R <sub>1</sub> , wR <sub>2</sub> (I > 2σI)	0.0460, 0.1092	0.0265, 0.0650	0.0582, 0.1271

is therefore reversible suggests that the two forms of 1 represent an enantiotropic system<sup>24</sup> in which the Z' = 1 polymorph is more stable at high temperature and the Z' = 2 form is the more stable at lower temperature. Other interesting features in the DSC include a glass transition ( $T_g = 149$  K) and a large crystallization exotherm followed by melting endotherm at 180 K which we believe is due to the crystallization and subsequent melting of surface sulphuric acid (concentrated H<sub>2</sub>SO<sub>4</sub> has a melting point of 276 K, but this value is very concentration dependent<sup>25</sup> and can go as low as ca. 180 K in ca. 35% aqueous solution) as the crystals are highly deliquescent. The glass transition is also likely to be associated with the sulphuric acid solution rather than the crystalline product.

X-ray data were collected at 120 K (1(LT)) and 140 K (1(HT)) on either side of the phase transition. Table 1 shows crystallographic parameters for the two data sets, and Figure 3 shows an overlay of the non-hydrogen atom positions in the two structure determinations.

It is clear from Figure 3 that the positions of the majority of non-hydrogen atoms do not change greatly in the two different forms. The most significant change is around the sulfate anion ringed in Figure 3 which is central to the hydrogen-bonded network. Because of the short contact between one of the oxygen atoms in the ringed sulfate ion and neighboring sulfate oxygen atom as well as a careful study of the S–O bond lengths in the ringed sulfate ion, we believe this is a hydrogen sulfate ion. We therefore postulate that the phase change is related to the strength and directionality of the hydrogen bonds within the sulfate/hydrogen sulfate/water network. This distinction cannot easily be made using X-rays as the data quality was not sufficient to locate all the hydrogen atoms in the lower-temperature phase. Neutron diffraction was therefore employed to ascertain the exact hydrogen atom positions. Neutron experiments on a large crystal of 1 were carried out using VIVALDI at the Institut Laue-Langvin in Grenoble, France.<sup>26,27</sup> The crystal was slow cooled to 120 K and a full data set was collected. The crystal was then warmed to 130 K after which Laue patterns were collected at 2 K intervals. The patterns were closely monitored for the disappearance of diffraction peaks which would indicate that the phase transition had occurred. According to the data collected, axis halving occurred between 140 K and 142 K, which, allowing for some hysteresis, is in agreement with the exotherm observed in the DSC and with the X-ray data. Figure 4 shows parts of patterns at the same sample orientation taken above and below the phase-change temperature showing the disappearance of peaks corresponding to the axis halving. The crystal was then warmed up to 144 K to ensure that the transition was fully complete and a full data set was collected.

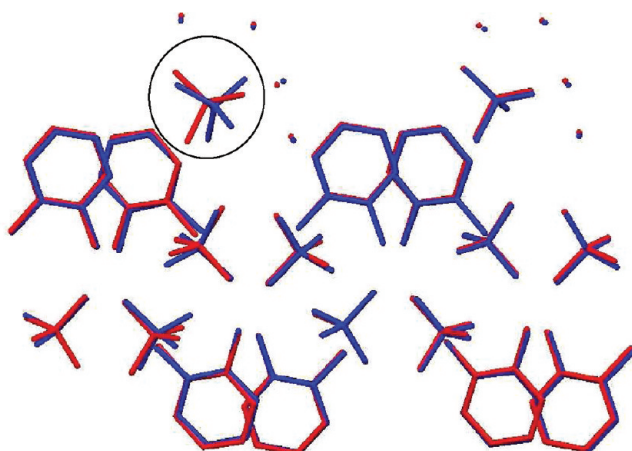


**Figure 3.** An overlay of 1(LT) (blue) and 1(HT) (red) viewed down the *a* axis. Half of the 1(HT) structure has been generated by symmetry.

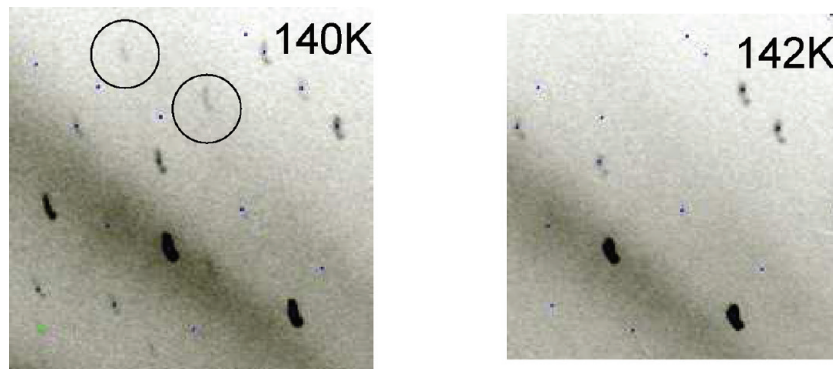
The crystals form as very large flat plates that are highly subject to multiple twinning and cracking parallel to the plane of the plate and hence the neutron data proved to be generally extremely challenging to interpret as evidenced by the nonregular spot shape seen in Figure 4. The resulting data are therefore not of the highest quality but are more than sufficient to locate the hydrogen atoms qualitatively, although some of the atomic parameters are not particularly precise. The accurate location of the hydrogen atoms gives rise to a slightly altered asymmetric unit formula for 1(LT), which is now formally (H<sub>2</sub>-o-PDA<sup>2+</sup>)<sub>8</sub>(H<sub>5</sub>O<sub>2</sub><sup>+</sup>)<sub>2</sub>(SO<sub>4</sub><sup>2-</sup>)<sub>8</sub>(HSO<sub>4</sub><sup>-</sup>)<sub>2</sub>·4H<sub>2</sub>O, and 1(HT), which is now formally (H<sub>2</sub>-o-PDA<sup>2+</sup>)<sub>4</sub>(H<sub>5</sub>O<sub>2</sub><sup>+</sup>)(SO<sub>4</sub><sup>2-</sup>)<sub>4</sub>(HSO<sub>4</sub><sup>-</sup>)·2H<sub>2</sub>O. Figure 5 shows the unique part of the water/hydrogen sulfate/sulfate hydrogen bonded network in the neutron structures of (a) 1(LT) and (b) 1(HT).

Table 2 shows O···O contact distances for the hydrogen bonds shown in Figure 5 derived from the X-ray data (which are more precise than the neutron data for the heavy atoms). The distances for 1(LT) are presented in two parts, 1(LT)<sub>1</sub> and 1(LT)<sub>2</sub> corresponding to the two unique hydrogen-bonded networks present in the structure (e.g., O16 in 1(LT)<sub>1</sub> corresponds to O36 in 1(LT)<sub>2</sub>).

Some O···O distances in 1(HT) lie between the two distances observed in the corresponding 1(LT) structure, suggesting that some domains of the 1(HT) structure are averages of the unsymmetrical parts of 1(LT). This averaging is not always the case, however, as some of the 1(HT) O···O distances lie outside the range observed in the two 1(LT) parts.

Several of the O···O distances in the two unsymmetrical portions of 1(LT) (i.e., 1(LT)<sub>1</sub> and 1(LT)<sub>2</sub>) differ significantly; for example, there is nearly 0.1 Å difference in the two O19···O12 distances (2.649(4) and 2.562(4) Å) compared with the difference of just 0.001 Å in the two O3W···O1W distances (2.538(4) and 2.539(4) Å) which are identical within experimental error. The fact that only some of these contact distances differ between the unsymmetrical portions again suggests that only part of the 1(LT) structure is affected by the phase change. Figure 6 shows an overlay of the unique part of the hydrogen-bonded network for the three independent networks, namely, 1(LT)<sub>1</sub> (red), 1(LT)<sub>2</sub> (black), and 1(HT) (blue).

It is clear from Figure 6 that the major difference in the three motifs is the hydrogen sulfate ion based on S(10) in 1(LT)<sub>2</sub>.



**Figure 4.** Neutron Laue patterns recorded at 140 and 142 K showing the disappearance of supercell reflections (circled). The small squares indicate the positions of the allowed reflections in 1(HT).

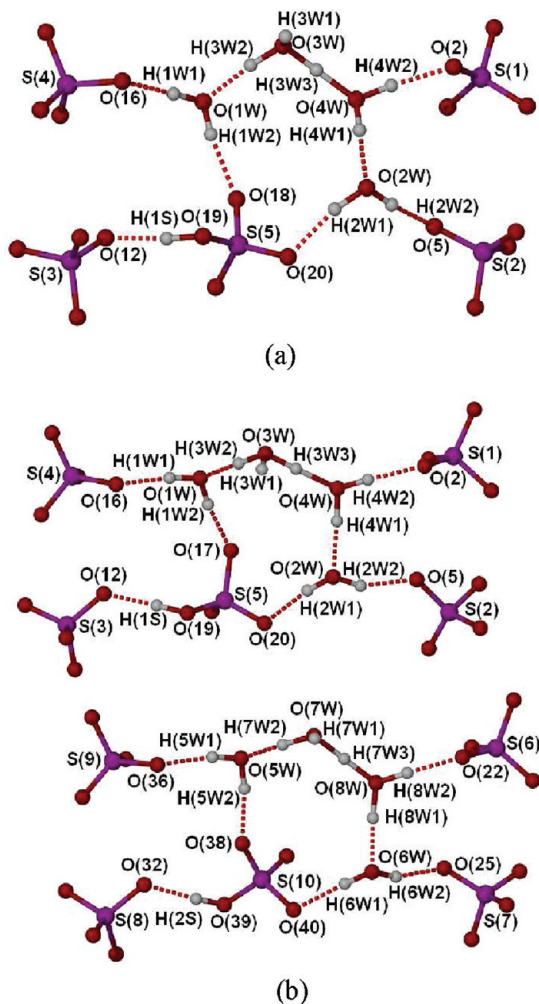


**Figure 5.** The unique part of the water/hydrogen sulfate/sulfate hydrogen bonded network in the neutron structures of (a) 1(HT) and (b) 1(LT).

The driving force for this change appears to be an increase in hydrogen-bond strength in the hydrogen sulfate to sulfate hydrogen bond  $\text{O}19 \cdots \text{O}12 (\text{SO}_4^{2-} \cdots \text{HOSO}_3^-)$  corresponding to a change in the  $\text{O} \cdots \text{O}$  distance from  $2.649(4)$  in 1(LT)<sub>1</sub> and  $2.590(3)$  in 1(HT) to  $2.562(4)$  in 1(LT)<sub>2</sub>.

**Table 2. O  $\cdots$  O Distances ( $\text{\AA}$ ) in the Hydrogen-Bonded Networks of 1(LT) and 1(HT) from X-ray Data<sup>a</sup>**

	1(LT) <sub>1</sub>	1(LT) <sub>2</sub>	1(HT)
O1W $\cdots$ O16	2.764(4)	2.761(4)	2.772(3)
O1W $\cdots$ O18 <sup>b</sup>	2.723(4)	2.688(4)	2.737(3)
O2W $\cdots$ O5 <sup>b</sup>	2.733(4)	2.731(4)	2.717(3)
O2W $\cdots$ O20 <sup>c</sup>	2.757(4)	2.786(4)	2.744(3)
O3W $\cdots$ O1W <sup>d</sup>	2.538(4)	2.539(4)	2.554(3)
O3W $\cdots$ O4W	2.428(4)	2.425(4)	2.421(3)
O4W $\cdots$ O2	2.753(4)	2.718(4)	2.704(3)
O4W $\cdots$ O2W	2.645(5)	2.598(4)	2.604(3)
O19 $\cdots$ O12	2.649(4)	2.562(4)	2.590(3)

<sup>a</sup>  $a = -1 + X, +Y, -1 + Z$ ,  $b = 1 + X, +Y, +Z$ ,  $c = 2 - X, -0.5 + Y, 1 - Z$ ,  $d = 1 - X, -0.5 + Y, -Z$ .

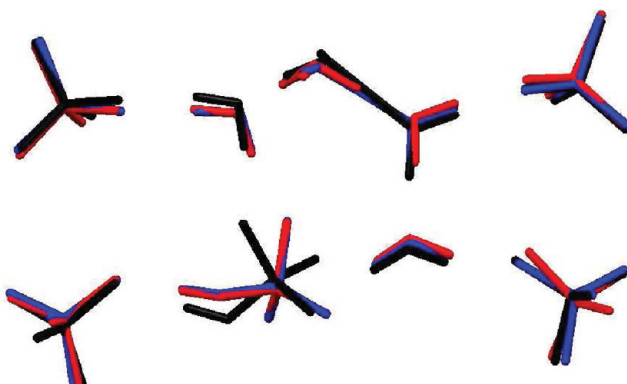
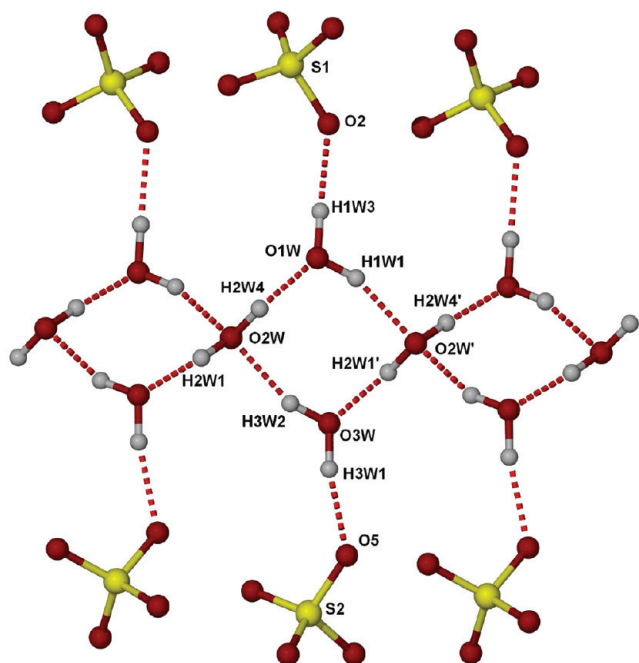


**Figure 6.** Overlay of the hydrogen-bonded portions of the three independent networks, 1(HT) (blue), 1(LT)<sub>1</sub> (red), and 1(LT)<sub>2</sub> (black).

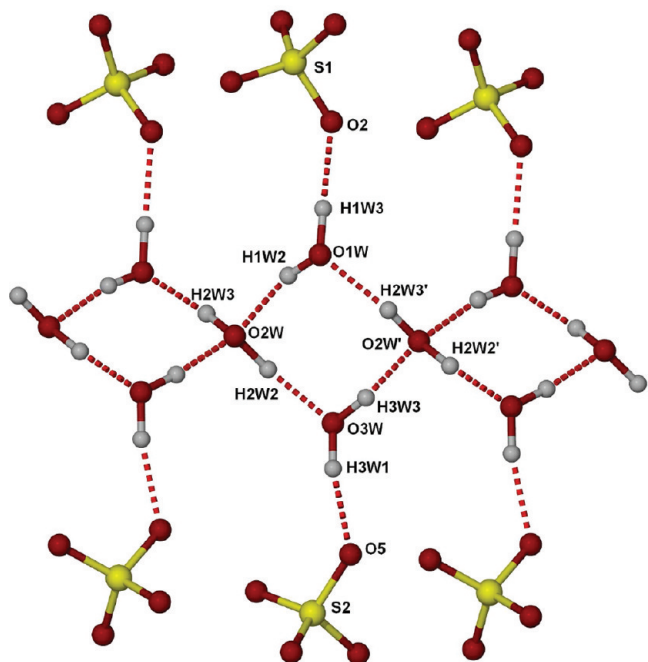
**Table 3. Selected O–H Bond Lengths from Neutron Data**

	1(LT) <sub>1</sub>	1(LT) <sub>2</sub>	1(HT)
O3W–H3W3	1.06(3)	1.19(3)	1.11(2)
O4W–H3W3	1.44(3)	1.25(3)	1.32(3)

Concomitantly, there is a proton shift around the  $\text{H}_2\text{O}_5^+$  ion; in 1(LT)<sub>1</sub> and 1(HT) hydrogen H3W3 is localized on O3W,



(a)



(b)

**Figure 7.** “Flip-flop” water chain in 2 showing (a) major (prime atoms  $x, 0.5 - y, 0.5 + z$ ) and (b) minor parts of the disorder (prime atoms  $x, 0.5 - y, z - 0.5$ ).

but in **1(LT)\_2** it moves to a position that is essentially halfway between O3W and O4W (Table 3). Even though crystal quality limits the Laue data precision, the qualitative nature of the change

**Table 4.** Hydrogen-Bond Parameters from Neutron Data in the Water Chain of 2

	D-H	H...A	D...A	D-H...A
Major Component				
O1W-H1W1...O2W	0.922(14)	1.936(13)	2.822(6)	160.4(11)
O2W'-H2W1'...O3W	0.961(13)	1.798(13)	2.755(5)	173.3(14)
O3W-H3W2...O2W	0.925(12)	1.923(12)	2.807(6)	159.4(12)
O2W-H2W4...O1W	0.962(10)	1.803(10)	2.763(6)	176.0(12)
Minor Component				
O1W-H1W2...O2W	0.86(3)	1.92(3)	2.763(6)	166(2)
O2W-H2W2...O3W	1.02(2)	1.79(2)	2.807(6)	173.9(19)
O3W-H3W3...O2W'	0.94(2)	1.82(2)	2.755(5)	171(2)
O2W'-H2W3'...O1W	0.96(3)	1.87(3)	2.822(6)	172(2)

**Table 5.** Hydrogen Bonds from Water to Sulfate Anions in 2

	D-H	H...A	D...A	D-H...A
O1W-H1W3...O2	0.967(7)	1.896(7)	2.859(5)	173.2(8)
O3W-H3W1...O5	0.951(8)	1.890(8)	2.828(5)	168.5(8)

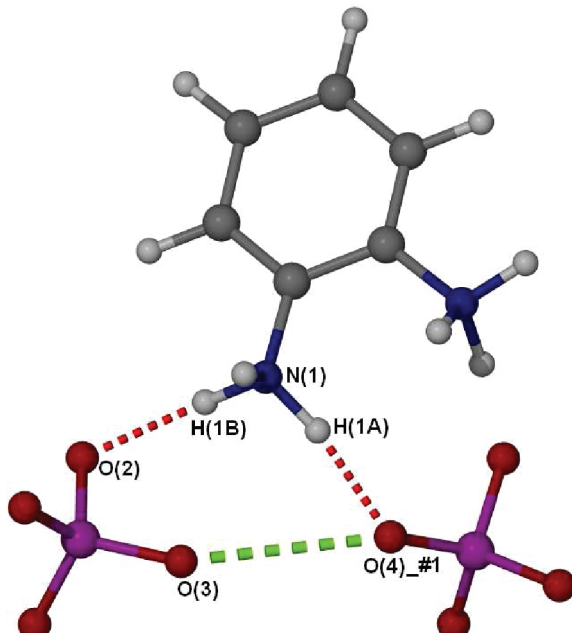


**Figure 8.** Short O...O contact (in green) and associated hydrogen bonds in 2. #1 =  $-X, -1/2 + Y, 1/2 - Z$ .

is clear not only from the hydrogen atom positions but also within the heavy-atom framework. We can thus say that in this enantiotropic system lowering the temperature places stricter directional constraints on the hydrogen-bonded network as the proton thermal motion decreases, leading to symmetry breaking and a more stable  $Z' = 2$  structure that can accommodate more linear hydrogen bonds.<sup>28</sup> At higher temperatures, the increased proton thermal motion places fewer constraints on the hydrogen-bonding network allowing a higher symmetry structure that minimizes unfavorable nonbonded contacts. The phase transition thus represents a conflict between the directional hydrogen

bonding (which wins out at low temperature) and efficient packing (which wins out at higher temperature).

**Neutron Study of  $(H_2\text{-}o\text{-PDA}^{2+})_2(SO_4^{2-})_2 \cdot 3H_2O$ .** If *o*-phenylenediamine is recrystallized from less acidic conditions, then a different compound  $(H_2\text{-}o\text{-PDA}^{2+})_2(SO_4^{2-})_2 \cdot 3H_2O$  (**2**) is formed. Compound **2** crystallizes with  $Z' = 1$  and  $Z'' = 7$  and has very similar unit-cell parameters to the higher-temperature form of **1** (Table 1). The X-ray structure of **2** has been determined previously<sup>29</sup> and was described as including a “flip-flop” water chain (a linked sequence of mutually orthogonal four-membered hydrogen-bonded rings) as well as helical chains of sulfate anions formed by noncovalent  $O \cdots O$  interactions with an  $O \cdots O$  distance of 2.9413(16) Å. The original report suggests that this intersulfate distance is “shorter than the sum of their van der Waals radii (rvdW: O, 1.52 Å) indicating a strong non-covalent  $O \cdots O$  interaction”. The proposed existence of attractive  $O \cdots O$  interactions between sulfate anions is surprising. Attractive  $O \cdots O$  interactions have been observed in neutral aromatic nitro derivatives<sup>30</sup> but are virtually unknown for anionic oxygen atoms such as those in sulfate anions. A CSD search for short (i.e., less than the van der Waals distance)  $O \cdots O$  contacts between sulfate anions shows fewer than 10 hits, the majority of which correspond to either highly disordered structures<sup>31</sup> or

those where the location of protons is unclear (and hence likely represent hydrogen-bonded hydrogen sulfate anions).<sup>32</sup> To study this suggested phenomenon further, we undertook a neutron diffraction study of **2** using the four-circle diffractometer D19 at the ILL in Grenoble.<sup>33,34</sup> The neutron structure determination gave good agreement with the heavy-atom positions found from the X-ray structure with the shortest sulfate  $\cdots$  sulfate  $O \cdots O$  nonbonded contact being 2.932(9) Å; however, location of the hydrogen atoms showed that there is disorder in the “flip-flop” water chain which has two orientations of hydrogen atoms with a 63:37 ratio. Figure 7 shows the (a) major and (b) minor components of the water chain. The water chain is linked to the sulfate anions via two strong  $O\text{-}H \cdots O$  hydrogen bonds (Table 5).

The neutron structure confirms that there are no hydrogen atoms in between the sulfate oxygen atoms involved in the short  $O \cdots O$  contacts, and hence this contact is not a hydrogen bond. In view of the number of strong hydrogen bonds in this structure and the connection between the strongly hydrogen-bonded water chain and the sulfate anions, we suggest that the  $O \cdots O$  short contacts observed between sulfate anions in **2** are an enforced repulsive short contact brought about by the strong, charge-assisted hydrogen bonding from the water and *o*-phenylenediammonium cations in other parts of the structure and represent an unfavorable contribution to an overall stable lattice. In particular, each short  $O \cdots O$  contact is bridged by one  $NH_3^+$  group and the neutron structure shows that the  $NH \cdots O$

**Table 6. Hydrogen Bonding in **2****

	D-H	H $\cdots$ A	D $\cdots$ A	D-H $\cdots$ A
N1-H1A $\cdots$ O4 <sup>1</sup>	1.030(9)	1.799(9)	2.801(5)	163.1(10)
N1-H1B $\cdots$ O2	1.030(11)	1.887(9)	2.878(5)	160.4(12)

<sup>a</sup>#1 =  $-X, -1/2 + Y, 1/2 - Z$ .

**Scheme 1. Amines Used to Produce Analogs of **1****

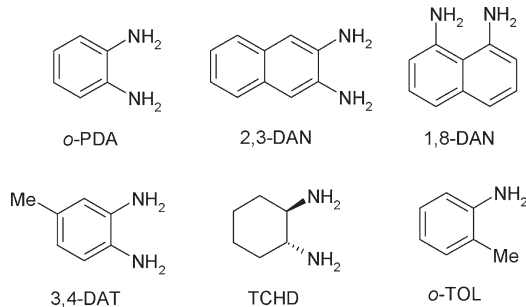


**Table 7. Summary of Structures **1**–**9b****

	amine	anion	other	$Z'$	density	2D/3D	face-face $\pi\text{-}\pi$	edge-face $\pi\text{-}\pi$	hydrogen bond saturation
<b>1</b>	<i>o</i> -PDA	$HSO_4^- / SO_4^{2-}$	$H_2O / H_3O^+$	4 or 8	1.631 (HT)	3D	Y	N	Y
					1.651 (LT)				
<b>2</b>	<i>o</i> -PDA	$SO_4^-$	$H_2O$	2	1.604	3D	N	N	Y
<b>3</b>	2,3-DAN	$HSO_4^-$		1/2	1.526	3D	N	N	Y
<b>4</b>	1,8-DAN	$HSO_4^-$		1	1.800	2D	Y	Y	N
<b>5</b>	3,4-DAT	$SO_4^{2-}$		1	1.587	2D	N	Y	Y
<b>6</b>	TCHD	$SO_4^{2-}$		1	1.508	2D			Y
<b>7</b>	<i>o</i> -TOL	$HSO_4^-$	$H_3O^+$	1	1.558	2D	Y	Y	Y
<b>8</b>	PhNH <sub>3</sub>	$HSO_4^-$	—	2	1.553	2D	Y	Y	Y
<b>9a</b>	<i>o</i> -TOL	$H_2PO_4^-$	$H_3PO_4$	1	1.541	2D	Y	N	Y
<b>9b</b>	<i>o</i> -TOL	$H_2PO_4^-$		4	1.390	2D	N	Y	Y

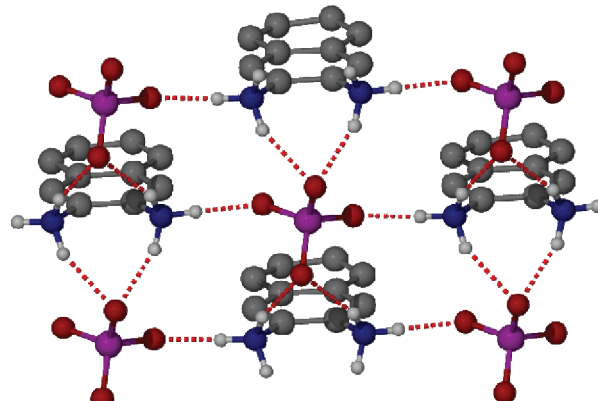


**Figure 9. Hydrogen-bonded network in **3**.**

interactions across this bridge are short and linear (Figure 8, Table 6). The existence of repulsive short contacts in charged hydrogen-bonded systems is well precedented.<sup>35–37</sup>

**Analogues of  $(H_2\text{-}o\text{-PDA}^{2+})_4(SO_4^{2-})_3(HSO_4^-)_2 \cdot 4H_2O$ .** It is clear from the structures of **1** and **2** that the intermolecular interactions play a large part in determining the overall crystal packing arrangement, and hence we were interested in the effect of varying the cation and, to a lesser extent the anion, on the structure of chemically related compounds. A series of different amines were chosen (Scheme 1), 2,3-diaminonaphthalene (2,3-DAN), 1,8-diaminonaphthalene (1,8-DAN), and 3,4-diaminotoluene (3,4-DAT) representing different degrees of potential  $\pi$ – $\pi$  stacking contributions while *trans*-diaminocyclohexane (TCHD) removes the  $\pi$ – $\pi$  stacking capability of the cation completely. We were also interested in the shape vs hydrogen bonding argument<sup>38</sup> so chose a derivative that has an almost

identical molecular shape to *o*-PDA but which is anticipated to exhibit weaker hydrogen bonding, namely, *o*-toluidine (*o*-TOL).

Starting amines were recrystallized from a mixture of concentrated sulfuric (1–8) or phosphoric acid (**9a,b**) and water. Table 7 shows a summary of the results obtained from the crystallizations which will be discussed in detail below. Each structure is examined against several criteria, first what the  $Z'$  value is, whether there is hydrogen-bond saturation (where the total number of donor hydrogen atoms exactly matches the number of acceptor lone pairs),<sup>39</sup> whether the cations are involved in  $\pi$ -stacking, and finally what the overall dimensionality of the hydrogen-bonded network is, principally whether the packing consisted of two-dimensional (2D) layers or 3D networks.

First, we were interested to see the effect of changing the  $\pi$ – $\pi$  stacking ability of the cation on the packing so two naphthalene derivatives were prepared using 1,2-diaminonaphthalene (2,3-DAN) and 7,8-diaminonaphthalene (1,8-DAN), Scheme 1. 2,3-DAN was recrystallized from a mixture of concentrated sulfuric acid and water giving tiny crystals. These were not suitable for determination using a laboratory X-ray source, so data were collected using synchrotron radiation on Station 9.8 at Daresbury. The crystals were very poor quality and gave split reflections consistent with twinning, but we were able to solve the structure which crystallizes as  $(H_2\text{-}2,3\text{-DAN}^{2+})(SO_4^{2-})$  (**3**) with  $Z' = 1/2$ . We are confident of correct space-group choice despite space-group absence violations, which are likely to be a result of the overlap of multiple diffraction patterns; however, no suitable twin law could be identified and as a result the residuals for the refinement are relatively high. With this in mind detailed structural parameters are not presented here, but we are confident that the data are good enough to characterize the general environment of the molecules. Despite the extended naphthalenyl  $\pi$ -surface, the naphthalene derived moieties do not  $\pi$ -stack; instead, they are arranged in an offset manner with the closest centroid–centroid distance around 6.6 Å. The absence of  $\pi$ -stacking seems to be a result of the optimization of the spacing required for the hydrogen bonding within the structure, as

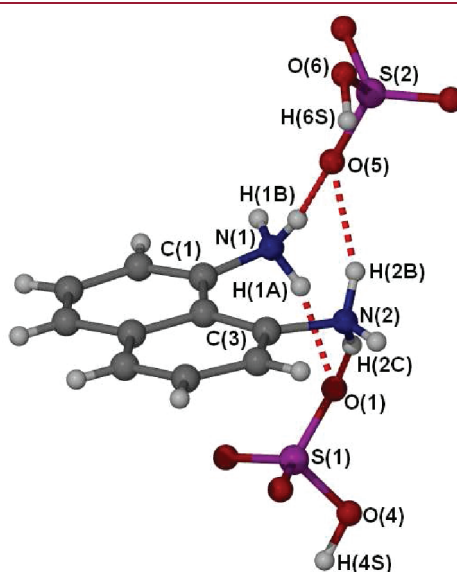


Figure 10. Asymmetric unit of **4** showing N–H...O hydrogen bonds.

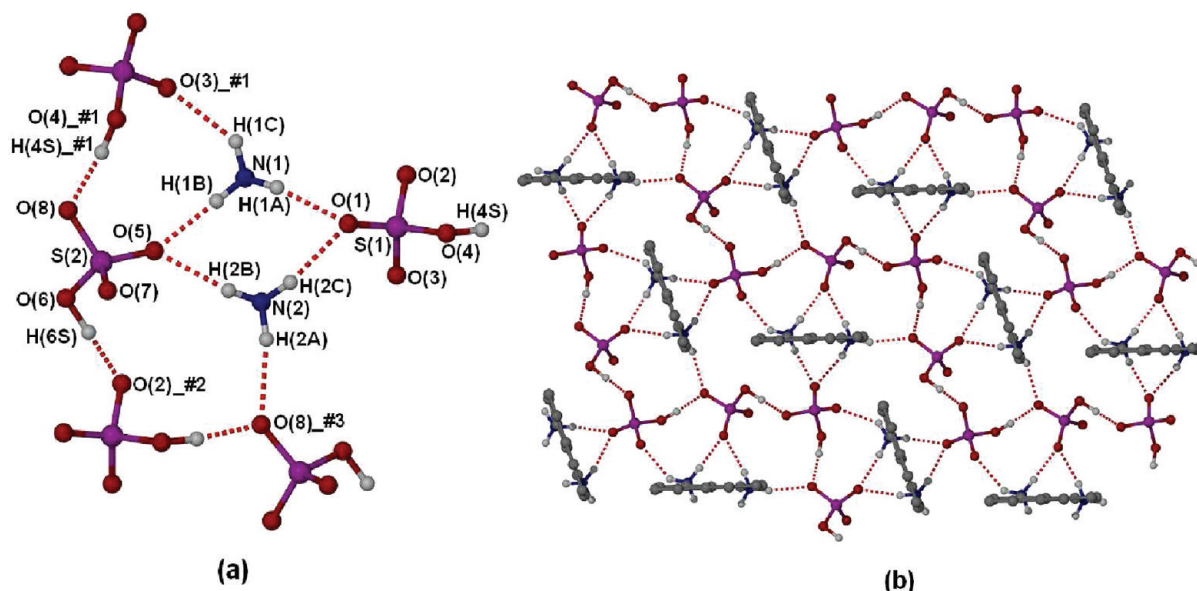


Figure 11. View down the  $a$  axis in **4** showing the hydrogen-bonded sheet (a) in detail and (b) an overview. The naphthalene-derived aryl backbone has been removed for clarity in (a). #1 =  $+X, 0.5 - Y, -0.5 + Z$ , #2 =  $+X, 1 + Y, +Z$ , #3 =  $+X, 1.5 - Y, 0.5 + Z$ .

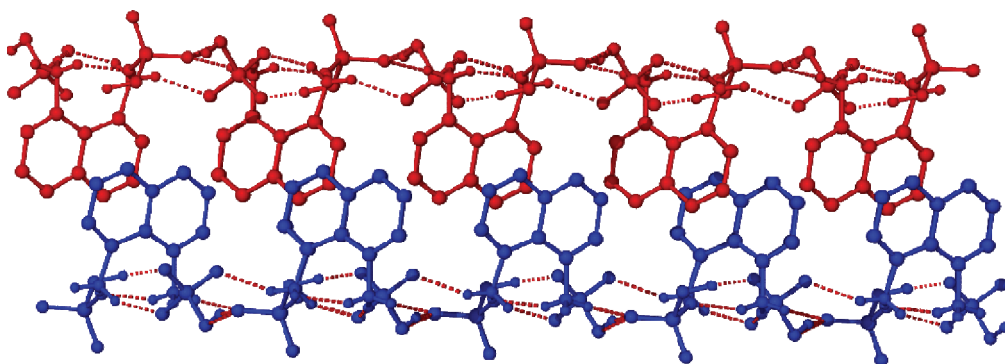


Figure 12. View down the  $b$  axis in 4 showing two layers.

Table 8. Hydrogen Bonding in 4<sup>a</sup>

	D–H <sup>b</sup>	H…A	D…A	D–H…A
O4 <sup>1</sup> –H4A <sup>1</sup> …O8	0.97	1.60	2.529(2)	159.4
O6–H6A…O2 <sup>2</sup>	1.03	1.52	2.553(2)	175.8
N1–H1B…O1	0.91	1.92	2.769(2)	154.3
N1–H1C…O5	0.91	1.91	2.800(3)	167.3
N1–H1A…O3 <sup>1</sup>	0.91	2.12	2.850(2)	136.0
N2–H2A…O1	0.91	1.99	2.872(3)	162.6
N2–H2B…O5	0.91	2.01	2.865(3)	156.6
N2–H2C…O8 <sup>3</sup>	0.91	2.04	2.936(2)	167.8

<sup>a</sup> #1 = +X, 0.5 – Y, –0.5 + Z, #2 = +X, 1 + Y, +Z, #3 = +X, 1.5 – Y, 0.5 + Z. <sup>b</sup> OH hydrogen atoms located experimentally but not refined.

packing this way ensures that the donors and acceptors are fully saturated and that the sulfate can accept six hydrogen bonds from the naphthalene N–H donors (Figure 9).

Using 1,8-DAN as a starting material gives a structure with formula ( $\text{H}_2\text{-1,8-DAN}^{2+}$ ) $(\text{HSO}_4^-)_2$  (4) and  $Z' = 1$  (Figure 10).

The ammonium hydrogen atoms and hydrogen sulfate anions are linked together via O–H…O and N–H…O hydrogen bonds to form a sheet with the pendant naphthalene-derived aryl groups all pointing in the same direction above the sheet (Figure 11). Detailed hydrogen-bonding information is given in Table 8.

The hydrogen-bond donors and acceptors in the structure are almost fully saturated with the exception of an S=O oxygen, O7, which does not undergo any hydrogen bonding and instead points perpendicular to the hydrogen-bonding plane into the space between the hydrogen-bonded sheets. The naphthalene molecules above the hydrogen-bonded sheet intercalate via  $\pi$ -stacking with naphthalene molecules in the sheet above to form a layer structure (Figure 12).

The doubly protonated 1,8-DAN molecules exhibit  $\pi$ -stacking between layers in both edge-to-face and face-to-face interactions (Figure 13), corresponding to a sandwich herringbone motif similar to that observed in pyrene.<sup>40–42</sup>

We were also interested in what would happen if the  $\pi$ -stacking in 1 was disrupted by addition of an extra group to the backbone of the aromatic ring so chose 3,4-diaminotoluene (3,4-DAT, Scheme 1) as a starting amine. Structural determination of the resulting crystals shows a  $Z' = 1$  structure with the same overall formula as 4, namely, ( $\text{H}_2\text{-3,4-DAT}^{2+}$ ) $(\text{HSO}_4^-)_2$  (5). The dication in 5 has the backbone methyl group disordered over two sites with an occupancy ratio of 56:44. The crystals were very small and plate-like leading to weak diffraction. There was also some evidence of twinning affecting

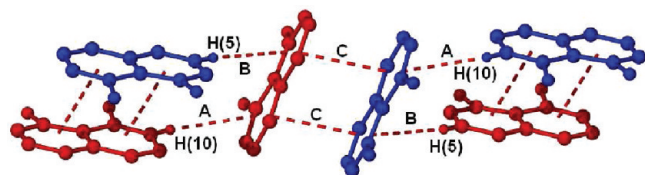


Figure 13.  $\pi$ – $\pi$  stacking observed between different layers in 4 with distances: A = 3.33 Å, B = 3.31 Å, C = 3.69 Å.

the  $c$  axis, but no suitable twin law could be found. Because of the problems with the diffraction data the two hydrogen sulfate protons could not be located in the difference map, but a study of the hydrogen-bonding pattern and S–O bond lengths indicates that the hydrogen atoms are located on O(3) and O(6). Compounds 4 and 5 are not isomorphous but are essentially isostructural as 5 also exhibits hydrogen-bonded sheets (Figure 14 and Table 9).

In this structure there is no  $\pi$ – $\pi$  stacking between layers (Figure 15) as this is presumably disrupted by steric hindrance resulting from the methyl group in the backbone; there are however some weak C–H… $\pi$  interactions (ca. 3.2 Å) involving only the minor position of the methyl group, and therefore these are not thought to be particularly significant. In light of this, it would appear that the hydrogen bonding in compounds 4 and 5 is the dominant (i.e., “structure determining”) interaction as 5 is isostructural despite the lack of  $\pi$ -stacking interactions and the presence of the methyl group.

We were therefore interested to see how similar the packing would be if the aromatic phenylenediamine was replaced by a saturated analogue, namely, *trans*-1,2-cyclohexanediamine (TCHD). Compound 6 crystallizes with formula ( $\text{H}_2\text{-TCHD}^{2+}$ ) $(\text{SO}_4^-)_2$  and has  $Z' = 1$ . Figure 16 shows the asymmetric unit viewed along the  $b$  axis. With  $\pi$ -stacking constraints removed, the only interaction of note is hydrogen bonding between the ammonium groups and the sulfate counterion. Two of the three ammonium hydrogen atoms participate in hydrogen bonds in the plane of the cyclohexane ring, which is in the chair conformation, while the remaining hydrogen participates in a hydrogen bond perpendicular to the plane linking the layers together. It is interesting to note that as in 5 the layer structure remains (Figures 17 and 18) despite the lack of  $\pi$ -stacking interactions. Hydrogen-bond parameters are shown in Table 10.

As hydrogen bonding is clearly a key feature of the structures observed thus far, we decided to leave the  $\pi$ -stacking component constant and instead change the hydrogen-bonding capabilities of the molecule. As we saw in 6, shape is also important and in order

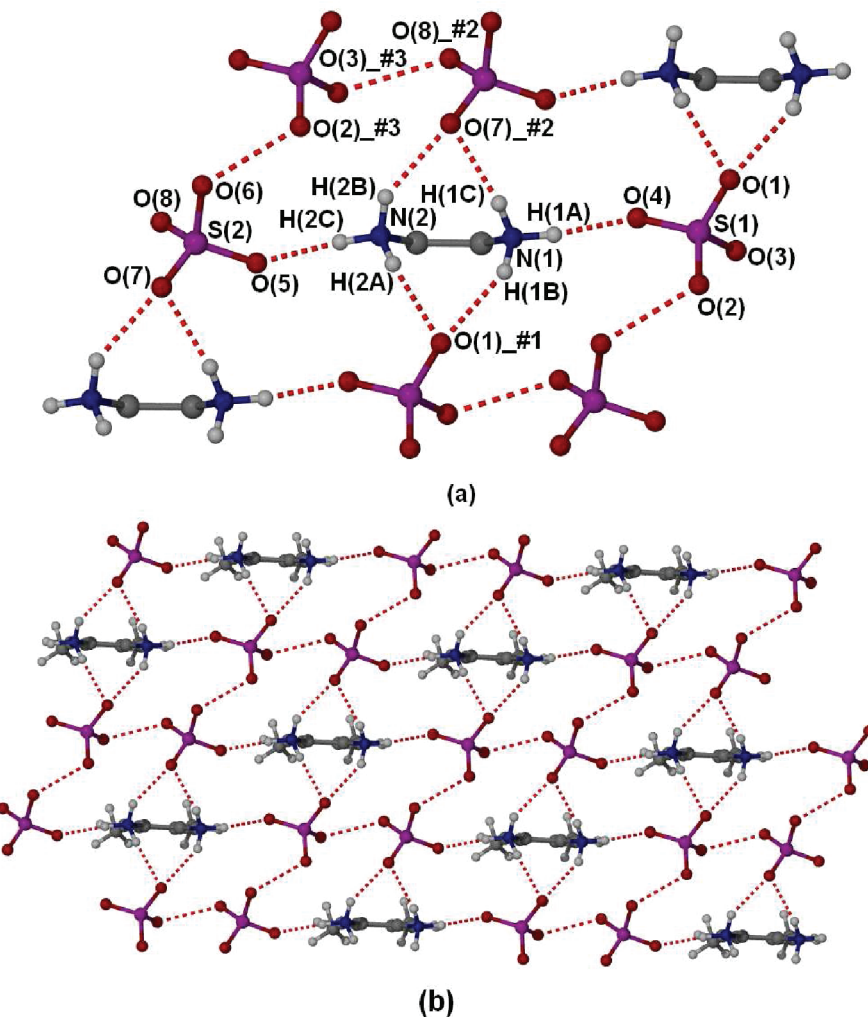


**Figure 14.** View down the *c* axis in **5** showing the hydrogen-bonded sheet (a) in detail and (b) an overview. The phenyl backbone has been removed for clarity in (a). #1 = 1 + *X*, +*Y*, +*Z*, #2 = −1 + *X*, +*Y*, +*Z*, #3 = 3 − *X*, 2 − *Y*, −*Z*.

**Table 9. Hydrogen Bonding in **4**<sup>a</sup>**

	D—H	H···A	D···A	D—H···A
N1—H1A···O4	0.91	1.88	2.789(5)	172.9
N2—H2C···O5	0.91	1.90	2.807(5)	174.4
N1—H1B···O1 <sup>1</sup>	0.91	2.11	2.891(5)	143.8
N1—H1C···O7 <sup>2</sup>	0.91	2.04	2.837(5)	146.0
N2—H2A···O1 <sup>1</sup>	0.91	2.05	2.849(5)	146.4
N2—H2A···O6 <sup>3</sup>	0.91	2.31	2.895(5)	122.0
O6···O2 <sup>3</sup>			2.509(5)	
O3 <sup>3</sup> ···O8 <sup>2</sup>			2.551(5)	

<sup>a</sup>#1 = +*X*, 0.5 − *Y*, −0.5 + *Z*, #2 = +*X*, 1 + *Y*, +*Z*, #3 = +*X*, 1.5 − *Y*, 0.5 + *Z*.

to keep as many parameters as consistent as possible, we decided to concentrate on *o*-toluidine (*o*-TOL, Scheme 1) as a starting material. This has essentially the same molecular shape as H<sub>2</sub>-*o*-PDA but with a methyl substituent replacing an ammonium group, although it is worth noting that the molecules are not directly comparable as the charge of the protonated versions is different.

Crystallization of *o*-TOL with a mixture of sulfuric acid and water leads to a structure with *Z'* = 1, namely, (H<sub>3</sub>O<sup>+</sup>)(H-*o*-TOL<sup>+</sup>)(SO<sub>4</sub><sup>2-</sup>) (7). The room temperature structure of 7 has been determined

previously,<sup>43</sup> but unlike the published structure we were able to locate and refine all of the oxonium protons at 120 K thus confirming the nature of the counteranion. Unsurprisingly in 7 the methyl hydrogen atoms do not participate in any intermolecular interactions and the packing is dominated by N—H···O and O—H···O hydrogen bonds (Figure 19). Hydrogen-bonding parameters are given in Table 11.

The packing in 7 is similar to the overall nature of the packing in **5** and **6** where the molecules are arranged in layers (Figure 20) with successive layers linked together by π-stacking interactions.

This layer structure with interlayer π-stacking is also seen in the previously reported crystal structure of the aniline-derivative anilinium hydrogen sulfate which crystallizes with formula (PhNH<sub>3</sub><sup>+</sup>)(HSO<sub>4</sub><sup>-</sup>) (8) and *Z'* = 2;<sup>21</sup> however, the π-stacking is slightly different between layers as shown in Figure 21.

Both 7 and 8 have one unique face-to-face π-stacking interaction and two equivalent C—H···π stacking interactions. The face–face interaction in 8 is shorter than that in 7 which may be due to steric hindrance by the methyl group in 7. However, the methyl group in 7 provides a much stronger C—H···π interaction which is nearly 1.5 Å shorter than the equivalent aryl-CH···π interaction in 8.

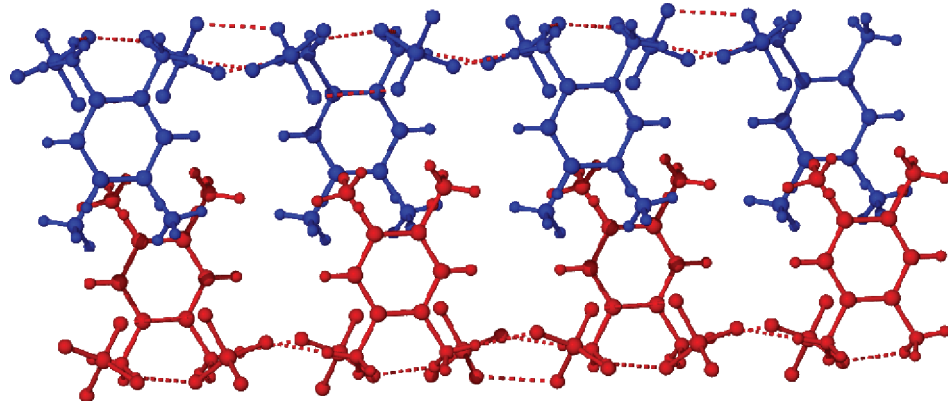
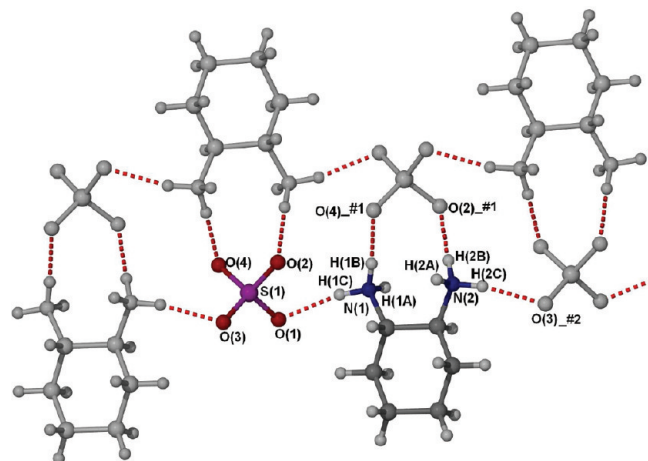
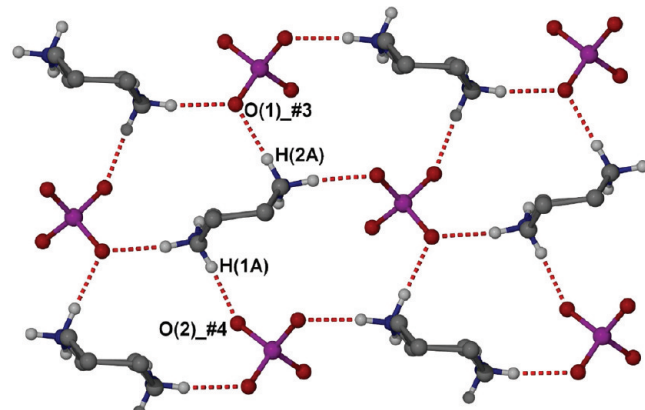
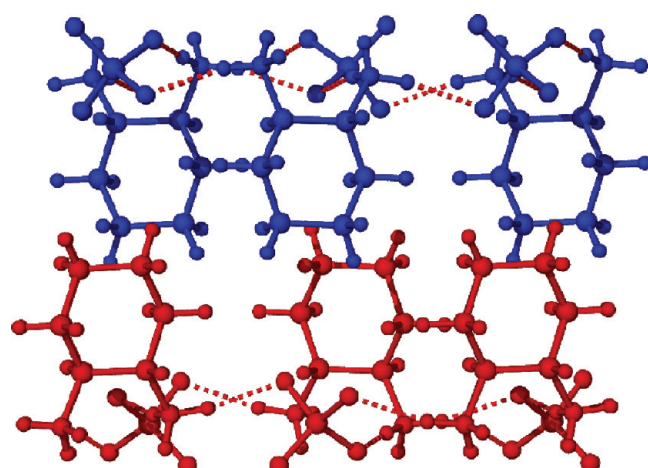


Figure 15. Layer structure of 5.

Figure 16. View showing the asymmetric unit of 6 (symmetrically generated molecules in gray). #1 =  $-1/2 + X, 1/2 - Y, 1 - Z$ , #2 =  $-1 + X, Y, Z$ .Figure 18. View down the  $c$  axis showing hydrogen-bonded sheet in 6. #3 =  $1/2 - X, 1/2 + Y, Z$ , #4 =  $1/2 - X, -1/2 + Y, Z$ .Figure 17. View down the  $b$  axis showing hydrogen-bonded layers in 6.

It is interesting to note the difference in composition of the formula unit between 7 and 8 despite the fact that there is only a small structural difference (a methyl group) between the two compounds. Neither compound seems able to crystallize with

Table 10. Hydrogen-Bonding Parameters for 9<sup>a</sup>

hydrogen bond	H $\cdots$ A	D $\cdots$ A	D-H $\cdots$ A
N1-H1A $\cdots$ O2 <sup>a</sup>	1.85	2.7586(18)	174
N1-H1B $\cdots$ O4 <sup>b</sup>	1.90	2.8104(17)	177
N1-H1C $\cdots$ O1	1.98	2.8701(17)	164
N2-H2A $\cdots$ O1 <sup>c</sup>	1.89	2.7866(17)	168
N2-H2B $\cdots$ O2 <sup>b</sup>	1.92	2.8226(18)	172
N2-H2C $\cdots$ O3 <sup>d</sup>	1.97	2.8656(18)	168

<sup>a</sup> a =  $1/2 - X, -1/2 + Y, Z$ , b =  $-1/2 + X, 1/2 - Y, 1 - Z$ , c =  $1/2 - X, 1/2 + Y, Z$ , d =  $-1 + X, Y, Z$ .

what would probably be predicted as the simplest form with just the monoprotonated cation and a hydrogen sulfate anion in the asymmetric unit; instead the H<sub>2</sub>-o-TOL cation crystallizes with a sulfate/oxonium mixture, and the protonated aniline has two of each cation and anion in the asymmetric unit, possibly suggesting that the Z' = 1 ArNH<sub>3</sub><sup>+</sup>/HSO<sub>4</sub><sup>-</sup> structure is not favorable.

As the anion clearly has a large effect on the hydrogen-bonding interactions, we next decided to look at the effect changing the anion has on the hydrogen bonding and hence the structure. Previously we had shown that crystallization of o-PDA from phosphoric acid gives a bis-dihydrogen phosphate salt with Z' = 1.<sup>21</sup> The packing in this structure is similar to that in 1,

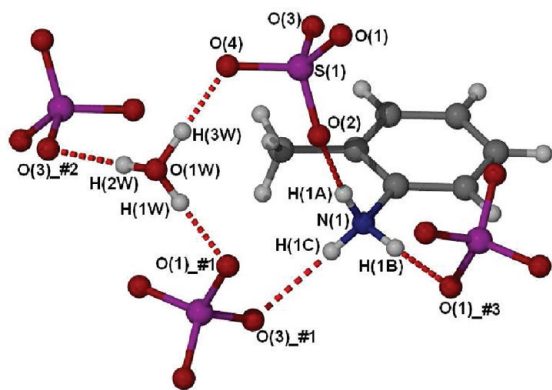


**Figure 19.** Hydrogen bonding in 7. #1 = +X, 0.5 – Y, 0.5 + Z, #2 = 1 – X, –Y, 2 – Z, #3 = 1 – X, 0.5 + Y, 1.5 – Z.

**Table 11. Hydrogen-Bond Parameters in 7**

	D–H	H···A	D···A	D–H···A
O1W–H1W···O1 <sup>1</sup>	0.85(2)	1.64(3)	2.4905(14)	178(2)
O1W–H2W···O3 <sup>2</sup>	0.82(3)	1.77(3)	2.5737(14)	171(2)
O1W–H3W···O4	0.94(2)	1.59(2)	2.5282(14)	179(2)
N1–H1B···O1 <sup>3</sup>	0.91	1.85	2.7391(15)	165.6
N1–H1A···O2	0.91	1.84	2.7367(15)	169.0
N1–H1C···O3 <sup>1</sup>	0.91	2.10	2.9990(16)	167.8

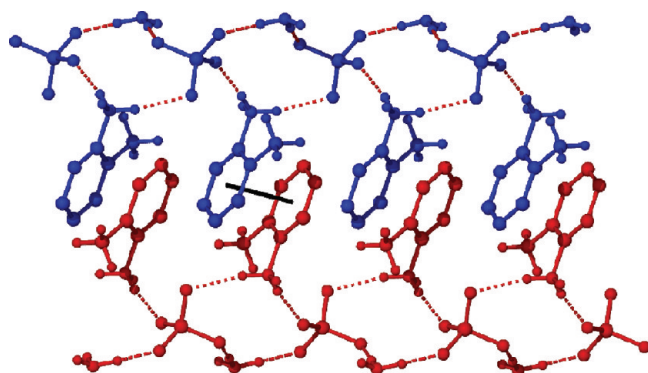


**Figure 20.** Two layers in 7 linked together by  $\pi$ -stacking interactions, centroid···centroid distance (in black) = 3.61 Å.

with the *o*-PDA molecules arranged in stacks surrounded by a 3D network of hydrogen-bonded phosphates.

Recrystallization of *o*-TOL from an aqueous solution of phosphoric acid gives two different crystal forms depending on the initial crystallization conditions, specifically how concentrated the acid solution is. The first form crystallizes with formula  $(\text{H-}o\text{-TOL})^+(\text{H}_2\text{PO}_4^-) \cdot \text{H}_3\text{PO}_4$  **9a** with  $Z' = 1$ , whereas if a lower concentration of phosphoric acid is used then crystals with the formula  $(\text{H-}o\text{-TOL}^{2+})(\text{H}_2\text{PO}_4^-)$  **9b** with  $Z' = 4$  are obtained.

Compound **9a** crystallizes as the dihydrogen phosphate salt cocrystallized with a neutral phosphoric acid molecule. This structure is known in the literature but only at room temperature. There is extensive hydrogen bonding in the structure with each donor and acceptor fully saturated (Figure 22 and Table 12).

The layer structure observed is very similar to the layer structure already seen for compounds of this type (Figure 23).

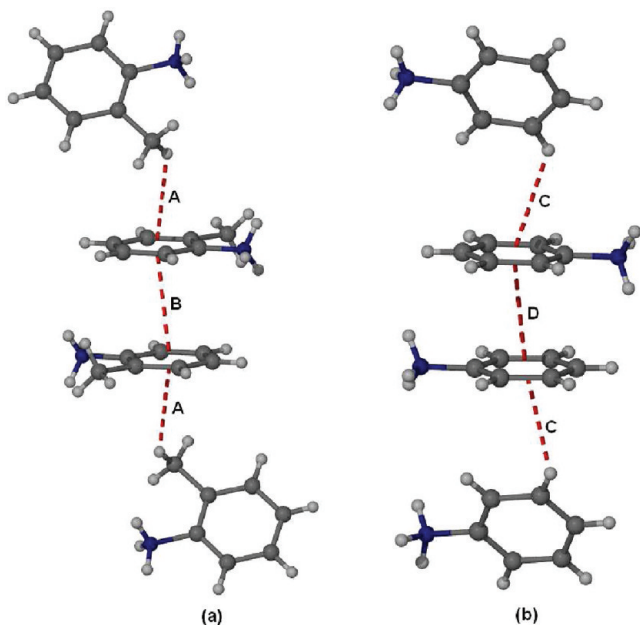


**Figure 21.**  $\pi$ -stacking in (a) 7 and (b) 8, centroid···centroid and C–H···centroid distances are A = 3.09 Å, B = 3.61 Å, C = 3.06 Å, D = 3.79 Å.

**Table 12. Hydrogen Bonds in **9a**<sup>a</sup>**

	D–H	H···A	D···A	D–H···A
N1–H1D···O4 <sup>2</sup>	0.91	2.03	2.932(2)	172.7
N1–H1E···O6 <sup>3</sup>	0.91	2.13	2.978(3)	155.0
N1–H1F···O1	0.91	1.88	2.770(2)	163.7
O2–H2O···O5 <sup>4</sup>	0.82(3)	1.79(3)	2.602(2)	172(3)
O4–H4O···O3 <sup>2</sup>	0.80(3)	1.84(3)	2.627(2)	167(3)
O6–H6O···O3 <sup>2</sup>	0.78(3)	1.73(3)	2.508(2)	174(3)
O7–H7O···O5 <sup>1</sup>	0.77(3)	1.85(3)	2.619(2)	177(3)
O8–H8O···O1 <sup>1</sup>	0.79(3)	1.74(3)	2.534(2)	175(4)

<sup>a</sup>#1 = 1 – X, –Y, 1 – Z, #2 = 1 – X, 0.5 + Y, 1.5 – Z, #3 = 1 – X, 1 – Y, 1 – Z, #4 = +X, 0.5 – Y, 0.5 + Z.

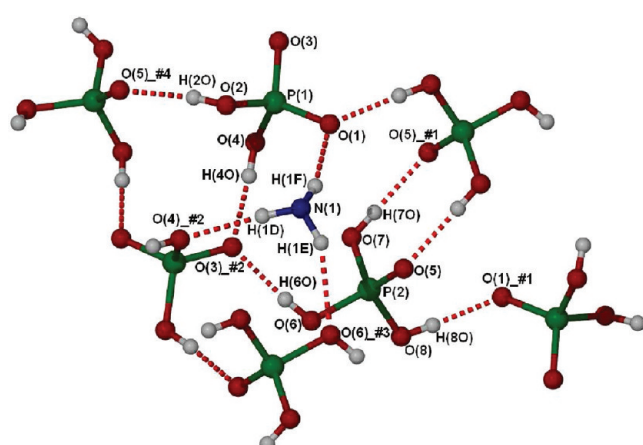


**Figure 22.** Hydrogen bonding in **9a**. Phenyl and methyl carbons and hydrogens have been removed for clarity. #1 = 1 – X, –Y, 1 – Z, #2 = 1 – X, 0.5 + Y, 1.5 – Z, #3 = 1 – X, 1 – Y, 1 – Z, #4 = +X, 0.5 – Y, 0.5 + Z.

with hydrogen-bonded layers linked together by  $\pi$ -stacking of the aromatic rings. There is a difference to the previously observed structures' however, in **9a** the hydrogen-bond layers are themselves hydrogen bonded together forming a continuous motif rather than the arrangements seen earlier in structures **4–8** where the hydrogen-bonded layers did not interact.

Between the layers the H-*o*-TOL<sup>+</sup> molecules are  $\pi$ -stacked in the same way as **8** albeit with a much larger centroid···centroid distance of 4.90 Å (cf. 3.79 Å in **8**); however, the C–H···centroid distance of 3.14 Å is shorter than in **8** (3.31 Å).

Compound **9b** crystallizes as the dihydrogen phosphate salt with an asymmetric unit consisting of four molecules of H-*o*-TOL<sup>+</sup> and four dihydrogen phosphate anions; hence  $Z' = 4$ . Two distinct hydrogen-bonded networks are formed, each containing two unique o-TOL<sup>+</sup> molecules and two dihydrogen phosphates (Figure 24). Again the molecules are arranged in layers, but in this instance there is no  $\pi$ -stacking between layers, only some weak C–H··· $\pi$  interactions (ca. 3.35–3.40 Å) involving methyl hydrogen atoms.

There is extensive hydrogen bonding within the layers with all donors and acceptors fully saturated (Figure 25); hydrogen-bond parameters are given in Table 13.

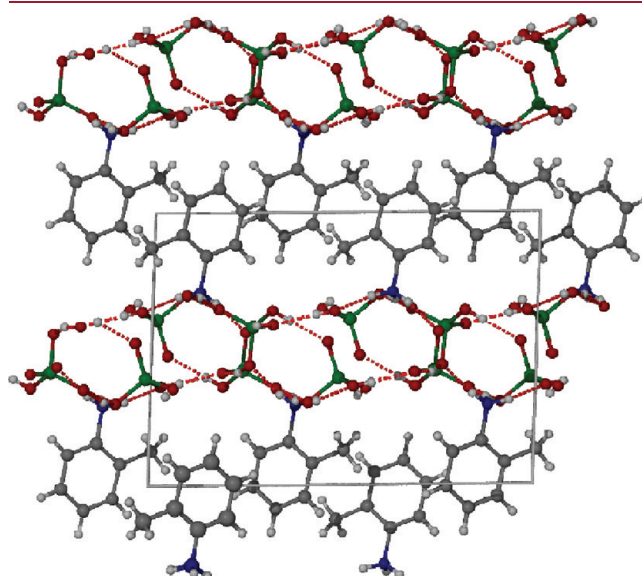


Figure 23. Layer structure in **9a**.

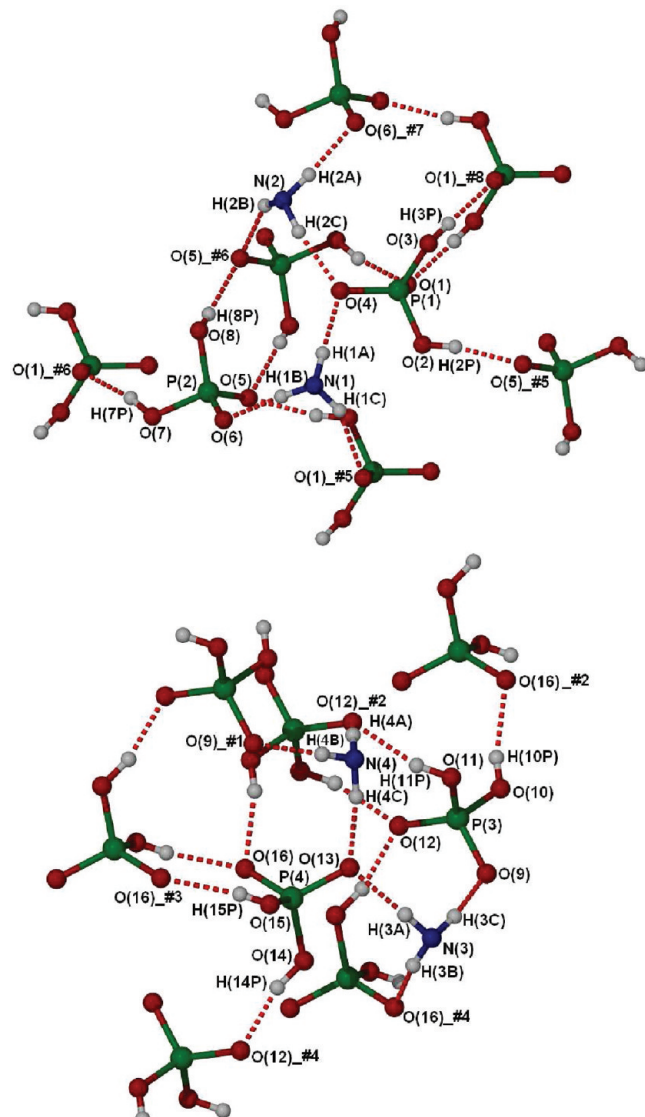


Figure 25. Hydrogen bonding in the two unique networks of **9b**. #1:  $+X, -1 + Y, +Z$ , #2:  $1 - X, 1 - Y, -Z$ , #3:  $2 - X, -Y, -Z$ , #4:  $2 - X, 1 - Y, -Z$ , #5:  $1 - X, 1 - Y, 1 - Z$ , #6:  $1 - X, -Y, 1 - Z$ , #7:  $1 + X, +Y, +Z$ , #8:  $2 - X, 1 - Y, 1 - Z$ .

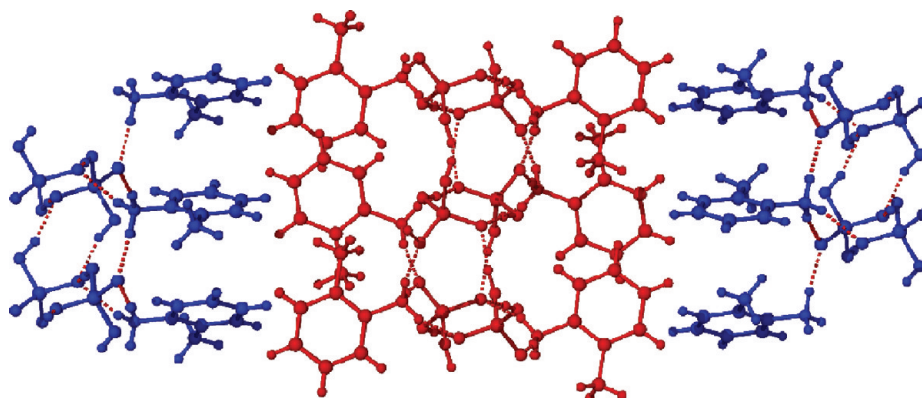


Figure 24. Layers in **9b**. The two distinct networks are colored red and blue and consist of two unique o-TOL<sup>+</sup> molecules and two dihydrogen phosphates.

**Table 13.** Hydrogen-Bond Parameters for **9b**<sup>a</sup>

	D–H	H···A	D···A	D–H···A
N4–H4B···O9 <sup>1</sup>	0.91	1.83	2.737(3)	175.0
N4–H4A···O12 <sup>2</sup>	0.91	2.03	2.857(3)	150.4
N4–H4C···O13	0.91	1.80	2.699(3)	171.0
O11–H11P···O12 <sup>2</sup>	0.85(4)	1.83(4)	2.650(3)	160(3)
O10–H10P···O16 <sup>2</sup>	0.74(5)	1.85(5)	2.577(3)	166(5)
O15–H15P···O16 <sup>3</sup>	0.73(4)	1.93(4)	2.647(3)	166(5)
N3–H3B···O9	0.91	1.80	2.701(3)	167.8
N3–H3A···O13	0.91	1.82	2.731(3)	176.2
N3–H3C···O16 <sup>4</sup>	0.91	2.02	2.861(3)	153.5
O14–H14P···O12 <sup>4</sup>	0.88(4)	1.71(4)	2.571(3)	166(4)
N1–H1C···O1 <sup>5</sup>	0.91	2.01	2.852(3)	153.2
N1–H1B···O4	0.91	1.81	2.719(3)	178.6
N1–H1A···O6	0.91	1.81	2.702(3)	165.9
O8–H8P···O5 <sup>6</sup>	0.70(4)	1.96(4)	2.648(3)	168(5)
O7–H7P···O1 <sup>6</sup>	0.93(5)	1.66(5)	2.575(3)	168(5)
N2–H2A···O4	0.91	1.81	2.704(3)	166.5
N2–H2B···O5 <sup>6</sup>	0.91	2.05	2.857(3)	147.7
N2–H2C···O6 <sup>7</sup>	0.91	1.81	2.716(3)	171.3
O2–H2P···O5 <sup>5</sup>	0.81(4)	1.78(4)	2.577(3)	165(4)
O3–H3P···O1 <sup>8</sup>	0.88(4)	1.77(4)	2.644(3)	170(4)

<sup>a</sup>#1: +X, -1 +Y, +Z, #2: 1 -X, 1 -Y, -Z, #3: 2 -X, -Y, -Z, #4: 2 -X, 1 -Y, -Z, #5: 1 -X, 1 -Y, 1 -Z, #6: 1 -X, -Y, 1 -Z, #7: 1 +X, +Y, +Z, #8: 2 -X, 1 -Y, 1 -Z.

The data in Table 6 suggest that hydrogen bonding plays a much more important role in determining the structures than  $\pi$ -stacking as witnessed by the fact that 9 of the 10 structures have a fully saturated hydrogen-bonding system, whereas only 7 of the 10 structures have some form of  $\pi$ -stacking. Layer structures feature heavily with only three of the compounds not featuring hydrogen-bonded layers. The layer structures observed may be a result of favoring the stacking of hydrophilic and hydrophobic regions. Four of the 10 structures (40%) have  $Z' > 1$ , which is a considerably larger proportion than observed for both the CSD as a whole (8.8%) and the value observed for ionic species (6.6%).<sup>21</sup> Two of the remaining five structures with  $Z' = 1$  (**7** and **9a**) contain additional molecules in the asymmetric unit, i.e., form cocrystals.<sup>44,45</sup> We have shown previously that molecules that crystallize with  $Z' > 1$  are good candidates for cocrystal formation,<sup>46</sup> and this seems to be the case here also. **9b** crystallizes as the dihydrogen phosphate salt with  $Z' = 4$ . If we consider the overall salt to be the “parent” molecule, then **9a** is the “child” cocrystal where an extra molecule, phosphoric acid, is included, and the value of  $Z'$  drops from 4 to 1.<sup>46</sup> None of the three remaining structures with  $Z' = 1$  have both face–face  $\pi$ – $\pi$  stacking interactions and a fully saturated hydrogen-bond system.

Compound **4** is interesting in that it is the only structure that does not have a fully saturated hydrogen-bond system, as one of the sulfate oxygen atoms does not participate in any hydrogen bonds nor is there any extra water included in the structure to compensate for this. It is clear that the interplay between hydrogen bonding and  $\pi$ -stacking is important in determining not only what the structure will actually look like but also what form is crystallized out of solution, i.e., whether it crystallizes with a dianion or two monoanions and/or whether there is any water in the structure. However, the extensive, charge-assisted hydrogen-bonding networks are the dominant feature in each case.

## CONCLUSION

Our studies have shown that charge-assisted hydrogen bonding is a very powerful tool in compounds containing protonated ammonium groups. Ensuring that the system is fully saturated,<sup>47</sup> that is, that all possible donors and acceptors participate in hydrogen bonds, is key in structure formation and often results in formation of structures with  $Z' > 1$  or cocrystallization with neutral molecules in order to achieve it. Bilayer-type structures with hydrophobic and hydrophilic regions are the most common motif, often with aromatic stacking between the hydrophobic part of the cations.

Other consequences of the dominance of an extensive network of charge-assisted hydrogen bonding within a structure are short repulsive contacts between oxygen atoms, as in **2**. We suggest that the short O···O are merely a result of maximizing the hydrogen-bonding strength and hence are an unfavorable contribution to an overall favorable energy.<sup>35–37</sup> We have also shown that small changes in the hydrogen bonded network can lead to symmetry breaking as in **1** where decreased proton movement and the consequent linearization of the hydrogen bond result in increased directional constraints and hence symmetry breaking and an increase in  $Z'$  from 1 to 2. The example of **1** shows that it is oversimplistic to regard either  $Z' = 1$  or  $Z' > 1$  forms as having any intrinsically greater stability. Instead, the crystal structure in general is a result of a balance in structural features in combination with nucleation and growth phenomena. The relative stability of polymorphs of a given substance with different  $Z'$  values is governed by the balance (or conflict leading to structural frustration) between competing factors. In this case, the  $Z' = 2$  structure arises from the linearization of the strong, charge-assisted hydrogen bonds at lower temperatures. Both forms are compatible with close packing, as attested by the higher density of the  $Z' = 2$  form.

## EXPERIMENTAL SECTION

Samples were prepared by recrystallizing the relevant amine from an acid solution using ~0.1 g of amine and a 10 mL/2 mL mix of water/concentrated acid unless otherwise stated. Specific experimental details can be found below:

**Compound 1.** Crystals suitable for both X-ray and neutron diffraction were grown from a solution containing 0.3159 g of *o*-phenylenediamine dissolved in a solution containing 3 mL of conc. sulfuric acid and 10 mL of water. Neutron diffraction studies were carried out on a crystal of approximate volume 2.4 mm<sup>3</sup> at the Institut Laue-Langevin, Grenoble, using the diffractometer very intense vertical axis Laue diffractometer (VIVALDI) with thermal neutron radiation ( $\lambda = 0.8\text{--}5.2 \text{ \AA}$ ). The VIVALDI instrument uses a cylindrical detector whose inner surface is lined with neutron-sensitive image plates to collect diffraction data over a solid angle of 8 sr and is especially suitable for small-molecule samples (primitive unit cells with cell lengths less than 25 Å). The sample was wedged between two wads of quartz wool inside a thin-walled silica glass tube and housed within a He-flow cryostat. Ten Laue patterns were recorded at each temperature at typically 20° intervals of rotation around an axis perpendicular to the incident neutron beam; the patterns at 120 K were recorded for 120 min each, while the patterns at other temperatures were recorded for 45 min each. The patterns were indexed using Lauegen of the CCP4 Laue suite.<sup>48</sup> Peak integration over the neutron Laue diffraction patterns was based on a 2D minimum  $\sigma(I)/(I)$  routine,<sup>49</sup> and the individual reflection intensities were normalized to a common wavelength by comparison of repeated observations including symmetry equivalents using an in-house program (Rearrange\_lam). X-ray diffraction studies were carried out on

Table 14. Crystal Data

	1(HT)	1(HT)	1LT	1LT	2	3	4	5	6	7	9a	9b
radiation	neutron	x-ray	neutron	x-ray	synchrotron	x-ray	x-ray	x-ray	x-ray	x-ray	x-ray	x-ray
formula	(H <sub>2</sub> -o-PDA <sup>2+</sup> ) <sub>4</sub> (SO <sub>4</sub> <sup>2-</sup> ) <sub>4</sub> (HSO <sub>4</sub> <sup>-</sup> ) (H <sub>2</sub> O <sub>5</sub> <sup>+</sup> ).2H <sub>2</sub> O	(H <sub>2</sub> -o-PDA <sup>2+</sup> ) <sub>4</sub> (SO <sub>4</sub> <sup>2-</sup> ) <sub>4</sub> (HSO <sub>4</sub> <sup>-</sup> ) (H <sub>2</sub> O <sub>5</sub> <sup>+</sup> ).2H <sub>2</sub> O	(H <sub>2</sub> -o-PDA <sup>2+</sup> ) <sub>4</sub> (SO <sub>4</sub> <sup>2-</sup> ) <sub>4</sub> (HSO <sub>4</sub> <sup>-</sup> ) (H <sub>2</sub> O <sub>5</sub> <sup>+</sup> ).2H <sub>2</sub> O	(H <sub>2</sub> -o-PDA <sup>2+</sup> ) <sub>2</sub> (SO <sub>4</sub> <sup>2-</sup> ) <sub>2</sub> .3H <sub>2</sub> O	(H <sub>2</sub> -1,8-DAN <sup>2+</sup> ) <sub>2</sub> (SO <sub>4</sub> <sup>2-</sup> ) <sub>2</sub>	(H <sub>2</sub> -3,4-DAT <sup>2+</sup> ) <sub>2</sub> (HSO <sub>4</sub> <sup>-</sup> ) <sub>2</sub>	(H <sub>2</sub> -TCHD <sup>2+</sup> ) <sub>2</sub> (SO <sub>4</sub> <sup>2-</sup> ) <sub>2</sub>	(H <sub>2</sub> O <sup>+</sup> )(H <sub>2</sub> -o-TOL <sup>+</sup> ) (H <sub>2</sub> PO <sub>4</sub> <sup>-</sup> ).H <sub>3</sub> PO <sub>4</sub>	(H <sub>2</sub> -o-TOL <sup>+</sup> ) (H <sub>2</sub> PO <sub>4</sub> <sup>-</sup> ).H <sub>3</sub> PO <sub>4</sub>	(H <sub>2</sub> -o-TOL <sup>+</sup> ) (H <sub>2</sub> PO <sub>4</sub> <sup>-</sup> ).H <sub>3</sub> PO <sub>4</sub>		
mass	995.02	995.02	995.02	466.36	274.29	354.35	318.32	212.27	223.24	303.14	205.15	
system	monoclinic	monoclinic	monoclinic	monoclinic	monoclinic	monoclinic	monoclinic	orthorhombic	orthorhombic	monoclinic	monoclinic	triclinic
a/Å	7.5904(4)	7.5816(3)	7.5816(3)	26.932(4)	9.5547(4)	8.4231(8)	7.4274(13)	9.6624(10)	9.3853(19)	10.8508(14)	8.161(3)	
b/Å	27.7714(15)	27.7714(15)	27.5580(12)	27.5580(12)	19.1638(8)	7.5226(2)	6.19(2)	13.7798(12)	12.706(2)	8.3157(9)	7.9002(10)	8.168(3)
c/Å	9.6134(5)	9.6134(5)	9.6134(5)	9.6134(5)	90.00	90.00	90.00	90.00	90.00	10.259(2)	15.2532(19)	29.607(10)
$\alpha/^\circ$	90.00	90.00	90.00	90.00	90.00	90.00	90.00	90.00	90.00	90.00	90.00	82.340(12)
$\beta/^\circ$	91.7530(10)	91.7530(10)	91.6150(10)	91.6150(10)	93.3313(13)	115.36(2)	105.312(3)	95.804(5)	90.00	90.00(3)	92.289(3)	85.463(14)
$\gamma/^\circ$	90.00	90.00	90.00	90.00	90.00	90.00	90.00	90.00	90.00	90.00	90.00	89.982(14)
V/Å <sup>3</sup>	2025.52(19)	2025.52(19)	4002.4(3)	4002.4(3)	1932.51(10)	1194(6)	1307.9(2)	666.01(19)	1870.4(3)	952.0(3)	1306.5(3)	1960.8(11)
temp/K	244(2)	240(2)	120(2)	120(2)	30(2)	120(2)	120(2)	120(2)	120(2)	120(2)	120(2)	120(2)
sp gr	<i>P</i> 2 <sub>1</sub>	<i>P</i> 2 <sub>1</sub>	<i>P</i> 2 <sub>1</sub>	<i>P</i> 2 <sub>1</sub> /c	C2/c	<i>B</i> 2 <sub>1</sub> /c	<i>P</i> 1	<i>P</i> bcac	<i>P</i> 1	<i>P</i> 2 <sub>1</sub> /c	<i>P</i> 2 <sub>1</sub> /c	
density	1.631	1.631	1.651	1.603	1.526	1.800	1.587	1.508	1.558	1.541	1.390	
Z, Z'	2, 1	2, 1	4, 2	4, 1	4, 0.5	4, 1	2, 1	8, 1	4, 1	4, 1	8, 4	
refls	15312	15207	21328	52002	20879	3060	8555	11217	15132	6505	11707	33465
measured												
indep refls	5953	6991	9078	18345	5537	1097	1867	3581	1351	2177	3489	10507
R <sub>int</sub>	0.2799	0.0240	0.2168	0.0438	0.1579	0.0565	0.0279	0.0689	0.0274	0.0331	0.0618	0.0431
R <sub>I</sub> ( $I >$ )	0.1172	0.0265	0.1411	0.0460	0.0903	0.1610	0.0267	0.0780	0.0242	0.0297	0.0455	0.0658
2σ( $I$ )												
wR(F <sup>2</sup> ) ( $I >$ )	0.1925	0.0650	0.2194	0.1092	0.1875	0.4520	0.0669	0.1921	0.0691	0.0781	0.0900	0.1330
2σ( $I$ )												
R <sub>I</sub> (all data)	0.1740	0.0301	0.2031	0.0658	0.1417	0.1732	0.0325	0.1151	0.0260	0.0328	0.0752	0.0868
wR(F <sup>2</sup> )	0.2006	0.0669	0.2283	0.1209	0.2377	0.4610	0.0699	0.2114	0.0703	0.0805	0.1003	0.1388
(all data)												

a Bruker diffractometer equipped with a SMART 6K CCD area detector and Oxford Cryostream N<sub>2</sub> cooling device, using graphite-monochromated Mo-K $\alpha$  radiation ( $\lambda = 0.71073 \text{ \AA}$ ).

**Compound 2.** A clear crystal, of approximate volume 14 mm<sup>3</sup> ( $3.4 \times 2.8 \times 1.4 \text{ mm}$ ), was mounted between two wads of quartz wool inside a thin-walled silica glass tube. This was glued onto an aluminum base, which was then mounted on a Displex cryorefrigerator on the ILL thermal-beam diffractometer D19 equipped with a very large horizontally curved position-sensitive detector. This detector is mounted symmetrically about the equatorial plane, with sample-to-detector distance of 76 cm, and subtends 30 deg vertically and 120 deg horizontally. It is based on multiwire gas counter technology. Readout of 256  $\times$  640 pixels per frame gives a nominal resolution of 0.12 deg vertically and 0.19 deg horizontally. The crystal was cooled slowly (2 K/min), while monitoring the diffraction pattern, to 30 K. The space group and the unit cell found by X-rays were confirmed at 30 K. The chosen neutron wavelength was 1.246(1)  $\text{\AA}$  from a Ge(115) monochromator in reflection (takeoff angle 70°). The accessible intensities, up to  $2\theta \leq 122.3^\circ$ , were measured, to preset monitor counts, in a series of typically 80°  $w$  scans, in steps of 0.07° and counting times of between 11.7 and 23.4 s per step. The average number of reflections per detector frame (i.e., at any one orientation) was on the order of 35. A range of crystal orientations (different  $\varphi$  and  $\chi$  positions) was used to explore as much reciprocal space as time permitted. Because of its large horizontal opening, only one detector position was required. Between the long scans, three strong or medium reflections were monitored about every 6 h in shorter scans and showed no significant change; the total measurement time at 30 K was 4.5 days. The unit-cell dimensions were calculated (ILL program Rafd19) at the end of the data collection, from the centroids in 3D of 6225 strong reflections ( $5.31 \leq 2\theta \leq 122.29^\circ$ ).

Bragg intensities were integrated in 3D using a version of the ILL program Retreat,<sup>48</sup> modified for the new detector geometry. For the 6225 strongest reflections, the mean positional errors for the centroids were 0.02°, 0.03°, and 0.07° (in the scan, horizontal and vertical directions, respectively). A total of 20881 Bragg reflections was obtained, of which 5538 were independent. The Bragg intensities were corrected for attenuation by the crystal (minimum and maximum transmission coefficients 0.4718 and 0.7327, ILL program D19abs) and for attenuation by the cylindrical inner vanadium Displex heat-shield (minimum and maximum transmission coefficients 0.9046 and 0.9675, ILL program D19abscan).

**Compound 3.** Diffraction data were collected at 120 K (5) on a Bruker SMART1000 CCD diffractometer equipped with an Oxford Cryosystems open-flow cryostat, employing synchrotron radiation ( $\lambda = 0.6900 \text{ \AA}$ ).

**Compound 4.** Structure determination was carried out on a Bruker APEX diffractometer equipped with an Oxford Cryostream N<sub>2</sub> cooling device, using graphite-monochromated Mo-K $\alpha$  radiation ( $\lambda = 0.71073 \text{ \AA}$ ).

**Compound 5.** Structure determinations were carried out on a Bruker diffractometer equipped with a SMART 6K APEX CCD area detector and Oxford Cryostream N<sub>2</sub> cooling device, using graphite-monochromated Mo-K $\alpha$  radiation ( $\lambda = 0.71073 \text{ \AA}$ ).

**Compound 6.** Structure determinations were carried out on a Bruker diffractometer equipped with a SMART 1K CCD area detector and Oxford Cryostream N<sub>2</sub> cooling device, using graphite-monochromated Mo-K $\alpha$  radiation ( $\lambda = 0.71073 \text{ \AA}$ ).

**Compound 7.** Crystallization was set up using a 1:10:10 (v:v:v) ratio of *o*-toluidine/water/conc. sulfuric acid. Structure determinations were carried out on a Nonius Kappa CCD diffractometer and Oxford Cryostream N<sub>2</sub> cooling device, using graphite-monochromated Mo-K $\alpha$  radiation ( $\lambda = 0.71073 \text{ \AA}$ ).

**Compound 9a.** Crystallization was set up using a 3:4:8 (v:v:v) ratio of *o*-toluidine/water/conc. phosphoric acid. Structure determinations

were carried out on a Bruker diffractometer equipped with a SMART 1K CCD area detector and Oxford Cryostream N<sub>2</sub> cooling device, using graphite-monochromated Mo-K $\alpha$  radiation ( $\lambda = 0.71073 \text{ \AA}$ ).

**Compound 9b.** Crystallization was set up using a 3:10:7 (v:v:v) ratio of *o*-toluidine/water/conc. phosphoric acid. Structure determinations were carried out on a Bruker diffractometer equipped with a SMART 6K CCD area detector and Oxford Cryostream N<sub>2</sub> cooling device, using graphite-monochromated Mo-K $\alpha$  radiation ( $\lambda = 0.71073 \text{ \AA}$ ).

## ■ ASSOCIATED CONTENT

**S Supporting Information.** Crystallographic information files. This material is available free of charge via the Internet at <http://pubs.acs.org>.

## ■ AUTHOR INFORMATION

### Corresponding Author

\*E-mail: [jon.steed@durham.ac.uk](mailto:jon.steed@durham.ac.uk).

### Present Addresses

<sup>†</sup>The Bragg Institute, ANSTO, New Illawarra Road, Lucas Heights NSW 2232, Australia.

## ■ ACKNOWLEDGMENT

We would like to thank the EPSRC for funding and Mr. W. Douglas Carswell for the DSC studies. We would also like to thank Prof. William Clegg and the National Crystallographic Service staff for collecting data on Compound 3.

## ■ REFERENCES

- (1) Steed, J. W. *CrystEngComm* **2003**, *5*, 169.
- (2) Anderson, K. M.; Steed, J. W. *CrystEngComm* **2007**, *9*, 328.
- (3) Desiraju, G. R. *CrystEngComm* **2007**, *9*, 91.
- (4) Bernstein, J.; Dunitz, J. D.; Gavezzotti, A. *Cryst. Growth Des.* **2008**, *8*, 2011.
- (5) Chattopadhyay, B.; Hemantha, H. P.; Narendra, N.; Sureshbabu, V. V.; Warren, J. E.; Hellwell, M.; Mukherjee, A. K.; Mukherjee, M. *Cryst. Growth Des.* **2010**, *10*, 2239.
- (6) Bond, A. D. *CrystEngComm* **2008**, *10*, 411.
- (7) Bishop, R.; Scudder, M. L. *Cryst. Growth Des.* **2009**, *9*, 2890.
- (8) Cruz-Cabeza, A. J.; Karki, S.; Fabian, L.; Friscic, T.; Day, G. M.; Jones, W. *Chem. Commun.* **2010**, *46*, 2224.
- (9) Day, G. M.; Cooper, T. G.; Cruz-Cabeza, A. J.; Hejczyk, K. E.; Ammon, H. L.; Boerriger, S. X. M.; Tan, J. S.; Della Valle, R. G.; Venuti, E.; Jose, J.; Gadre, S. R.; Desiraju, G. R.; Thakur, T. S.; van Eijck, B. P.; Facelli, J. C.; Bazterra, V. E.; Ferraro, M. B.; Hofmann, D. W. M.; Neumann, M. A.; Leusen, F. J. J.; Kendrick, J.; Price, S. L.; Misquitta, A. J.; Karamertzanis, P. G.; Welch, G. W. A.; Scheraga, H. A.; Arnautova, Y. A.; Schmidt, M. U.; van de Streek, J.; Wolf, A. K.; Schweizer, B. *Acta Crystallogr. Sect. B* **2009**, *65*, 107.
- (10) Karamertzanis, P. G.; Kazantsev, A. V.; Issa, N.; Welch, G. W. A.; Adjiman, C. S.; Pantelides, C. C.; Price, S. L. *J. Chem. Theo. Comput.* **2009**, *5*, 1432.
- (11) Anderson, K. M.; Goeta, A. E.; Steed, J. W. *Cryst. Growth Des.* **2008**, *8*, 2517.
- (12) Babu, N. J.; Nangia, A. *CrystEngComm* **2007**, *9*, 980.
- (13) Das, D.; Banerjee, R.; Mondal, R.; Howard, J. A. K.; Boese, R.; Desiraju, G. R. *Chem Commun.* **2006**, 555.
- (14) Chandran, S. K.; Nangia, A. *CrystEngComm* **2006**, *8*, 581.
- (15) Caira, M. R.; Nassimbeni, L. R.; Su, H.; Weber, E. *CrystEngComm* **2003**, *5*, 351.
- (16) Coelho, A. C.; Amarante, T. R.; Klinowski, J.; Goncalves, I. S.; Paz, F. A. A. *Acta Crystallogr. Sect. E - Struct. Rep. Online* **2008**, *64*, O237.

- (17) Wilson, C. C.; Shankland, N.; Florence, A. J. *J. Chem. Soc.-Faraday Trans.* **1996**, 92, 5051.
- (18) Anderson, K. M.; Afarinkia, K.; Yu, H. W.; Goeta, A. E.; Steed, J. W. *Cryst. Growth Des.* **2006**, 6, 2109.
- (19) Allen, F. H.; Kennard, O. *Chem. Des. Autom. News* **1993**, 8, 31.
- (20) Allen, F. H. *Acta Crystallogr., Sect. B* **2002**, 58, 380.
- (21) Anderson, K. M.; Goeta, A. E.; Hancock, K. S. B.; Steed, J. W. *Chem. Commun.* **2006**, 2138.
- (22) van Eijck, B. P.; Kroon, J. *Acta Crystallogr., Sect. B* **2000**, 56, 535.
- (23) In our previous communication, this was recorded as a  $Z' = 8$  structure based on the number of independent cations as the location of the hydrogen atoms was ambiguous.
- (24) Bernstein, J. *Polymorphism in Molecular Crystals*; Oxford University Press: Oxford, U.K., 2008.
- (25) Rossa, L.; Vogtle, F. *Top. Curr. Chem.* **1983**, 113, 1.
- (26) Wilkinson, C.; Cowan, J. A.; Myles, D. A. A.; Cipriani, F.; McIntyre, G. J. *Neutron News* **2002**, 13, 37.
- (27) McIntyre, G. J.; Lemée-Cailleau, M. H.; Wilkinson, C. *Physica B* **2006**, 385–86, 1055.
- (28) Calleja, M.; Mason, S. A.; Prince, P. D.; Steed, J. W.; Wilkinson, C. *New J. Chem.* **2003**, 27, 28.
- (29) Raghavaiah, P.; Supriya, S.; Das, S. K. *Chem. Commun.* **2006**, 2762.
- (30) Wozniak, K.; He, H. Y.; Klinowski, J.; Jones, W.; Grech, E. *J. Phys. Chem.* **1994**, 98, 13755.
- (31) Ishida, T.; Ibe, S.; Inoue, M. *J. Chem. Soc., Perkin Trans. 2* **1984**, 297.
- (32) Kim, J.; Jung, I. S.; Kim, S. Y.; Lee, E.; Kang, J. K.; Sakamoto, S.; Yamaguchi, K.; Kim, K. J. *Am. Chem. Soc.* **2000**, 122, 540.
- (33) Mason, S. A.; Forsyth, V. T.; Howard, J. A. K.; Davidson, M. G.; Fuller, W.; Myles, D. A. In *Opportunities for Neutron Scattering in the 3rd Millennium*; Dianoux, J., Ed.; Institut Laue-Langevin: Grenoble, France, 2001, p 332.
- (34) Thomas, M.; Stansfield, R. F. D.; Berneron, M.; Filhol, A.; Greenwood, G.; Jacob, J.; Feltin, D.; Mason, S. A. In *Position-Sensitive Detection of Thermal Neutrons*; Convert, P., Forsyth, J. B., Eds.; Academic Press: London, 1983, p 344.
- (35) Braga, D.; D’Oria, E.; Grepioni, F.; Mota, F.; Novoa, J. J.; Rovira, C. *Chem.—Eur. J.* **2002**, 8, 1173.
- (36) Wood, P. A.; McKinnon, J. J.; Parsons, S.; Pidcock, E.; Spackman, M. A. *CrystEngComm* **2008**, 10, 368.
- (37) Price, S. L.; Stone, A. J.; Lucas, J.; Rowland, R. S.; Thornley, A. E. *J. Am. Chem. Soc.* **1994**, 116, 4910.
- (38) Angeloni, A.; Crawford, P. C.; Orpen, A. G.; Podesta, T. J.; Shore, B. *J. Chem.-Eur. J.* **2004**, 10, 3783.
- (39) Etter, M. C. *Acc. Chem. Res.* **1990**, 23, 120.
- (40) Desiraju, G. R.; Gavezzotti, A. *Acta Crystallogr. Sect. B* **1989**, 45, 473.
- (41) Desiraju, G. R.; Gavezzotti, A. *J. Chem. Soc., Chem. Commun.* **1989**, 621.
- (42) Gavezzotti, A.; Desiraju, G. R. *Acta Crystallogr. Sect. B* **1988**, 44, 427.
- (43) Gubin, A. I.; Khakimzhanova, G. D.; Nurakhmetov, N. N.; Erkasov, R. S.; Buranbaev, M. Z. *Kristallografiya* **1990**, 35, 1568.
- (44) Vishweshwar, P.; McMahon, J. A.; Bis, J. A.; Zaworotko, M. J. *J. Pharm. Sci.* **2006**, 95, 499.
- (45) Bond, A. D. *CrystEngComm* **2007**, 9, 833.
- (46) Anderson, K. M.; Probert, M. R.; Whiteley, C. N.; Rowland, A. M.; Goeta, A. E.; Steed, J. W. *Cryst. Growth Des.* **2009**, 9, 1082.
- (47) Loehlin, J. H.; Franz, K. J.; Gist, L.; Moore, R. H. *Acta Crystallogr.* **1998**, B54, 695.
- (48) Campbell, J. W.; Hao, Q.; Harding, M. M.; Nguti, N. D.; Wilkinson, C. *J. Appl. Crystallogr.* **1998**, 31, 496.
- (49) Wilkinson, C.; Khamis, H. W.; Stansfield, R. F. D.; McIntyre, G. J. *J. Appl. Crystallogr.* **1988**, 21, 471.